

Revealing the diversity of Type IIn supernova progenitors through their environments

ZEXI NIU ,^{1, 2} NING-CHEN SUN,^{1, 2, 3} EMMANOUIL ZAPARTAS ,^{4, 5} CONOR L. RANSOME ,⁶ JUSTYN R. MAUND ,⁷ CESAR ROJAS-BRAVO ,^{1, 2} AND JIFENG LIU^{2, 1, 3, 8}

¹*School of Astronomy and Space Science, University of Chinese Academy of Sciences, Beijing 100049, People's Republic of China*

²*National Astronomical Observatories, Chinese Academy of Sciences, Beijing 100101, China*

³*Institute for Frontiers in Astronomy and Astrophysics, Beijing Normal University, Beijing, 102206, People's Republic of China*

⁴*Institute of Astrophysics, Foundation for Research and Technology-Hellas, GR-71110 Heraklion, Greece*

⁵*Physics Department, National and Kapodistrian University of Athens, 15784 Athens, Greece*

⁶*Steward Observatory, University of Arizona, 933 N. Cherry Street, Tucson, AZ 85721, USA*

⁷*Department of Physics, Royal Holloway, University of London, Egham, TW20 0EX, United Kingdom*

⁸*New Cornerstone Science Laboratory, National Astronomical Observatories, Chinese Academy of Sciences, Beijing 100012, People's Republic of China*

ABSTRACT

Type IIn supernovae (SNe IIn) are hydrogen-rich explosions embedded in dense circumstellar medium (CSM), which gives rise to their characteristic narrow hydrogen emission lines. The nature of their progenitors and pre-explosion mass loss remains, however, poorly understood. Using high-resolution Hubble Space Telescope (HST) imaging, we analyze the local stellar environments of a volume-limited sample ($z < 0.02$) of 31 SNe IIn. The environments of SNe IIn are found to be very diverse; the SN could reside within a star-forming region (*Class 1*), outside a star-forming region (*Class 2*), or in much older environments without any obvious signs of star formation (*Class 3*). The bright SNe IIn ($M_{\text{peak}} < -19.5$ mag) predominantly occur in Class 1 environments, indicative of very massive progenitors, while the faint SNe IIn ($M_{\text{peak}} < -15.5$ mag) are associated with Classes 2 and 3 environments, suggesting the least massive progenitors. Meanwhile, normal SNe IIn with $-19.5 < M_{\text{peak}} < -15.5$ mag occur in all three types of environments, suggesting a diversity in their progenitor mass, lifetime, and evolutionary pathways. Moreover, the directly detected SN IIn progenitors are systematically brighter and/or bluer than the youngest stellar populations in their environments, suggesting that they were either in a non-quiescent state when observed or had experienced binary interactions. These results point to a significantly diverse origin for progenitors of SNe IIn, spanning a wide range of masses, evolutionary stages, and potential binary interaction histories.

1. INTRODUCTION

Type IIn supernovae (SNe IIn), characterized by narrow hydrogen (H) emission lines in their spectra (Schlegel 1990), constitute a fascinating yet enigmatic class of stellar explosions. Their defining observational features are attributed to the strong interaction between the expanding ejecta and a dense, pre-existing circumstellar medium (CSM). This interaction gives rise to a remarkable diversity in their observed properties, including light curves that span a wide range of peak luminosities, durations, and morphologies (e.g., Kiewe et al. 2012; Nyholm et al. 2020). The origin of the

dense CSM, usually requiring enhanced mass loss ($\dot{M} > 10^{-3} M_{\odot} \text{ yr}^{-1}$) in years to thousands of years preceding core collapse (Moriya et al. 2014), remains a key question in stellar astrophysics. Addressing this question relies on understanding the progenitor systems of SNe IIn, yet both the nature of the progenitor and the underlying explosion are often concealed behind the dense CSM interaction. Several scenarios have been proposed, including (1) core-collapse explosions of very massive stars, whose dense CSM may result from violent pre-SN eruptions or from binary-induced mass loss (Woosley et al. 2007; Smith et al. 2007); (2) core-collapse explosions of moderately massive stars, where the CSM is primarily shaped by binary interactions such as mass transfer or mergers (Smith & Arnett 2014; Soker & Kashi 2013); (3) thermonuclear explosions of lower-mass stars (white

dwarfs) within a dense, ejected common envelope (Jerkstrand et al. 2020).

Direct detections for progenitors of clearly confirmed SNe IIn in pre-explosion images have been limited. In the few cases where progenitors have been identified, they are consistently very luminous and blue, often exhibiting significant photometric variability, which are commonly reminiscent of luminous blue variable stars (LBVs; Gal-Yam et al. 2007; Smith et al. 2011b,a). Traditionally, LBVs are considered as a short-lived transitional phase for the most massive single stars ($M_{\text{ini}} > 30\text{--}40 M_{\odot}$) on their way to becoming Wolf-Rayet (WR) stars. The dense CSM observed for SNe IIn can thus be naturally interpreted by the enhanced wind and/or giant outburst similar to those seen from local LBVs (Humphreys & Davidson 1994; Humphreys et al. 1999). However, the direct explosion of LBVs is inconsistent with the traditional view (the Conti scenario, Conti & Alschuler 1971; see also Heger et al. 2003), and it is unclear whether all SNe IIn progenitors, especially those without direct detections, resemble LBVs prior to the explosion. Alternatively, the high luminosity of the detected progenitors could be attributed to pre-SN outbursts (e.g., Cheng et al. 2024), or the uncertain evolutionary pathways such as binary mergers (e.g., Justham et al. 2014).

Another powerful approach to constraining progenitors of core-collapse SNe is to analyze their local stellar environments. The principle is that massive stars ($M_{\text{ini}} > 8 M_{\odot}$) form in groups and share similar ages and metallicities, and they have short lifetimes and remain close to their birth sites. Since this technique does not rely on serendipitous pre-explosion images, it significantly enlarges the sample of SNe IIn available for analysis. It also helps to avoid biases introduced by precursor outbursts (Ofek et al. 2014), the self-obscuration of LBVs (Wachter et al. 2010), and the potentially wide range of intrinsic luminosities among progenitors. Moreover, the physics of the evolution of most surrounding stars, in particular those on the main sequence is generally better understood than the nature of the presumed LBV progenitors. Using pixel statistics techniques, SNe IIn have been found to have a similar association with star formation to the overall SNe II(P) population and red supergiants (RSGs), which are weaker than that of Type Ic SNe and LBVs (Anderson & James 2008; Anderson et al. 2012; Habergham et al. 2014; Kangas et al. 2017). Studies based on spatially resolved spectroscopy yield similar results, showing comparable environments for SNe IIn and SNe II in terms of metallicity and H α equivalent width (Pessi et al. 2025; Xi et al. 2025). These findings challenge the conventional

view that SNe IIn originate exclusively from very massive progenitors.

Furthermore, a key insight emerges from recent works that the SNe IIn environments are very diverse: some are linked to young stellar populations, tracing the high-mass progenitors, while others associated with old stellar populations, indicative of moderately massive progenitors (Galbany et al. 2018; Ransome et al. 2022; Xiao et al. 2023). Particularly, some SNe IIn, such as SN 2010jl, align well with very young star-forming regions (Niu et al. 2024), while others like SN 2009ip are located in a very sparse and old environments (Smith et al. 2016), which is inconsistent with the LBV progenitor of $50\text{--}80 M_{\odot}$ as inferred from the direct detection (see also (Smith et al. 2022) for a possible obscured young stellar cluster). These works come into a growing evidences pointing toward significant diversity among SNe IIn progenitors.

Most previous studies relied on comparative analyses between different types of SNe and massive stars, rather than directly characterizing the stellar populations surrounding SNe IIn. Recent work by Moriya et al. (2023) has explored the environmental dependence of SNe IIn using the integral field spectroscopy of their host galaxies, finding tentative correlations between SN properties and local interstellar conditions like metallicity and specific star formation rate. On the other hand, high-resolution imaging from the Hubble Space Telescope (HST) enables direct measurements of stars in the SN vicinity, providing powerful constraints on their ages and masses (Maund 2018; Sun et al. 2023). However, systematic studies of SNe IIn environments utilizing HST data as well as comparisons between the detected progenitors and their local stellar populations remain limited.

In this paper, we present a systematic study of local environments of 31 SNe IIn. We utilize a volume-limited sample ($z < 0.02$) observed with high-resolution HST imaging to ensure that the physical scales of star-forming complexes, crucial for understanding the local environments, are spatially resolved. We focus on the diversity of their environments, and its connections to SN properties, as well as comparisons between the progenitors and environmental stellar populations. This paper is structured as follows. Section 2 describes the sample selection and data reduction. We present the three classes of SNe IIn local environments in Section 3. In Section 4, we map the environmental dependence to infer possible progenitor channels and mass-loss mechanisms for SNe IIn of different luminosities. In Section 5, we infer the pre-explosion state of the progenitors by

comparing them with local stellar populations. We summarize our conclusions in Section 6.

2. DATA

2.1. SNe IIn sample

We started with the SNe IIn compilation provided by Habergham et al. (2014); Ransome et al. (2021, 2022); Ransome & Villar (2025); Hiramatsu et al. (2024). While discrepancies exist among these catalogs due to the complex nature of Type IIn SNe and heterogeneous community data sources, they encompass nearly all documented SNe IIn by the end of 2023. We note that a few spectroscopically confirmed SNe IIn from individual studies were excluded in the above references. These objects are included in our work (SN 2016jbu, Brennan et al. 2022a; SN 2010bt, Elias-Rosa et al. 2018; SN 2010jp, Smith et al. 2012). The classification of SN 1961V has been historically debated, between a true SN IIn and an SN impostor (i.e. non-terminal explosions of massive stars; Chu et al. 2004; Kochanek et al. 2011; Van Dyk & Matheson 2012). Recent evidence supports the core-collapse interpretation (Patton et al. 2019), and we therefore retain it in our sample. While some transients exhibit narrow emission lines in their spectra similar to those of SN IIn, they more closely resemble SN impostors or intermediate-luminosity red transients (e.g., SN 2008S and NGC 300OT; Berger et al. 2009; Cai et al. 2021). These transients are also not included in this work.

We further required $z < 0.02$, where stellar populations in the SN environments are spatially resolved in HST high-resolution imaging. Following an HST archive search (query date 2025-06-26), we retained 31 SNe IIn that have been observed by at least one broadband filter with either the Ultraviolet-Visible channel (UVIS) of Wide Field Camera 3 (WFC3) or the Wide Field Channel (WFC) of Advanced Camera for Surveys (ACS).

For SNe within 10 Mpc, we adopted the Cepheid distances of their host galaxy when available (SNe 1961V, 1997bs, 1978K, Kochanek et al. 2011; Van Dyk & Matheson 2012; Adams & Kochanek 2015; Chiba et al. 2020). For other SNe, we adopted Hubble distances assuming $H_0 = 73.3 \text{ km s}^{-1} \text{ Mpc}^{-1}$ (Riess et al. 2022). All distances for the whole sample are listed in Table 1.

2.2. HST photometry

Flat-fielded files (`*_f1c.fits` or `*_flt.fits`) were retrieved via the Mikulski Archive for Space Telescopes (MAST)¹, as listed in Table A1. Observations with ex-

posures at only a single point (i.e. not taken with a series of offsets) were excluded due to inadequate cosmic-ray removal. We combined the dithered exposures using the ASTRODRIZZLE package to remove cosmic rays and create drizzled science images, which served as reference frames for subsequent photometry. Point-spread-function (PSF) photometry was performed with the DOLPHOT package² (Dolphin 2000, 2016). The parameters `FitSky=2` and `RAper = 3` were applied. All other parameters followed recommendations in the DOLPHOT User’s Guide.

To ensure all sources are stellar, we selected those with `object type = 1`. We also applied the following criteria to identify resolved point sources in each filter:

- (1) `signal-to-noise ratio` ≥ 5 ;
- (2) $-0.5 \leq \text{sharpness} \leq 0.5$;
- (3) `crowding` ≤ 2 ;
- (4) `quality flag` ≤ 2 .

Artificial stars were randomly inserted to quantify and account for additional photometric uncertainties arising from source crowding and imperfect sky subtraction.

2.3. Pinpointing the SN locations

The SN positions on the HST images were carefully determined. Several SNe have had their explosion sites or progenitors identified within HST imaging, including SN 1961V (Kochanek et al. 2011; Patton et al. 2019), SN 1997bs (Van Dyk et al. 1999, 2000), SN 1998S (Mauerhan & Smith 2012), SN 1999el (Li et al. 2002), SN 2005gl (Gal-Yam et al. 2007), SN 2005ip (Fox et al. 2020), SN 2006gy (Fox et al. 2015), SN 2009ip (Smith et al. 2022, 2010), SN 2010bt (Elias-Rosa et al. 2018), SN 2010jl (Smith et al. 2011b; Niu et al. 2024), SN 2015bh (Elias-Rosa et al. 2016), SN 2016jbu (Kilpatrick et al. 2018), and SN 2021adxl (Brennan et al. 2024). These HST images served as our astrometric reference frames. For SN 1978K (Ryder et al. 1993), SN 2008J (Taddia et al. 2012), SN 2010jj (Schulze et al. 2021), SN 2013gc (Reguitti et al. 2019), and SN 2015bf (Lin et al. 2021), we used post-explosion imaging obtained from ground-based telescopes to determine the SN site. We performed astrometric transformations as detailed in Niu et al. (2025). The uncertainties of transformation were typically < 1 pixels for HST-to-HST alignments and 2–4 pixels for ground-based-telescope-to-HST alignments. At the distances of our SN sample, 1 HST pixel corresponds to 1–15 pc. For SN 2017hcc, it was still bright on the HST images analyzed in this work, from which we directly obtained the

¹ <https://mast.stsci.edu>

² <http://americano.dolphinsim.com/dolphot/>

SN position. For all other SNe, we validated the WCS using the python package TWIRL (Lang et al. 2010; Garcia et al. 2022) with *Gaia* reference stars. The resulting uncertainties were comparable to those from ground-based-telescope-to-HST transformations.

3. THREE CLASSES OF SN ENVIRONMENTS

For each SN, we constructed a stellar surface density map within an 800×800 pc region centered on the SN position. The map was generated by binning the resolved point sources into a two-dimensional histogram and convolving it with a Gaussian kernel to obtain a smoothed density map (Z_{smooth}). The kernel width represents the spatial resolution of the density map; a larger width suppresses noise at the expense of spatial details, while an overly small width introduces noise. Because the SNe in our sample span a range of distances and have been observed with different HST bands and exposure times, we adopted an empirical approach to set the width (Gouliermis et al. 2017; Sun et al. 2017). After testing a range of kernel sizes, we found that using the median distance to the 5th-nearest neighbor as the width provides an optimal balance between resolution and noise. The adopted width typically lie between 30 and 100 pc.

From a smoothed density map, the 3σ density enhancement contour corresponds to pixels with:

$$Z_{\text{smooth}} > m + 3\sigma \quad (1)$$

where the median m of the map was calculated via sigma-clipped statistics. Figures 1, 2, and 3 demonstrate representatives of SNe IIn environments in our sample. Orange iso-density contours mark the 3σ density enhancements, and these overdensities trace star-forming regions that have not been dissipated. Figures for the whole SNe IIn sample are in Appendix B.

We determined the projected distance to the nearest 3σ contour as the Euclidean distance from the SN position to the nearest point on any 3σ contour (i.e., the edge of the nearest star-forming regions). If the SN position fell inside a closed contour, the projected distance was set to zero.

Based on the local surface density map and the measured distances, we divide 31 SNe IIn into three classes:

Class 1 : The projected distance is less than 50 pc. The threshold of 50 pc accounts for the typical astrometric uncertainties and the smoothing introduced by the kernel. SNe of this class are likely to have very young and massive progenitors, although chance alignments cannot be entirely ruled out. An example is shown in Figure 1.

Class 2 : The projected distance is between 50 and 300 pc. The upper limit of 300 pc corresponds to the

projected distance within which approximately 90% of massive runaway stars from binary systems are predicted to be found (Renzo et al. 2019; Wagg et al. 2025). The Class 2 events may originate either from older stellar environments or from massive stars that have migrated from the adjacent star-forming complex. A representative case is displayed in Figure 2.

Class 3 : The projected distance is greater than 300 pc. These SNe are located far from any significant stellar overdensity and most probably arise from an older, more dispersed stellar population. An illustration is given in Figure 3.

We take special considerations for SNe 2009ip, 2010jp, 2015bf, 2017hcc, and Gaia14ahl. Smith et al. (2022) points that the nearly constant UV flux at the SN 2009ip site after a decade indicates a possible underlying young star cluster (< 10 Myr) behind the SN. Corgan et al. (2022) reports an likely extended H α emission behind the SN 2010jp, and they propose that it is related to a recent star formation with at least one late O-type star. Based on these indicators of recent star-forming activity, we reclassify these two SNe into Class 1, even though their environments appear sparse in HST resolved stellar photometry. SN 2017hcc remained significantly bright in 2021; the radius of the region that exceeds the background brightness by 5σ is approximately 0.14", corresponding to an obscured region with a radius of 48 pc at the SN distance. Due to the limited depth of the observations of the region hosting SN 2017hcc (see Appendix Figure C), we cannot rule out the presence of a compact obscured star-forming region. For SN 2015bf and Gaia14ahl, a noticeable enhancement in surface brightness is observed, yet fewer than 10 resolved stars were detected within 800 pc of these SNe. We suggest that this is likely due to the very shallow detection limits of the observations, which were conducted solely in the UV band. Thus, we reclassified them into Class 1. Although the possibility of Class 2 cannot be entirely excluded, this would not affect our main conclusions, as discussed in the following sections.

While the above reconsideration aims to provide a more physically complete picture of the local environment of SNe IIn in our sample, it introduces a potential inhomogeneity with respect to the remainder of the sample, which is classified based on the HST stellar density maps. We note that similar situations could, in principle, affect other SNe IIn in our sample. For example, some apparently sparse environments might host obscured star-forming regions that are not detected in the available optical HST images due to dust extinction or insufficient depth. Our HST-based classification

should be regarded as a conservative estimate that may underestimate the presence of young stellar populations.

The classifications for the whole sample are listed in Table 1. We identify 16 SNe as Class 1, 7 SNe as Class 2, and 8 SNe as Class 3. This highlights the diversity of environments of SNe IIn and is in agreement with the previous (Ransome et al. 2022). This diversity argues against very massive stars as the sole progenitor channel for SNe IIn (if that were the case, all SNe IIn would be of Class 1, or even Class 2 if progenitors have migrated). This suggests that SNe IIn progenitors should have multiple evolutionary pathways, with a range of initial masses and lifetimes.

4. RELATION WITH THE SN PEAK MAGNITUDES

In this section, we explore links between the properties of SN explosions and their environments. First of all, we need to identify a key parameter to characterize the SN explosion. CSM interaction is the dominating power source of SN IIn light curves; the complex nature of CSM introduces a considerable diversity, including a wide range of peak magnitudes, lasting timescale, rise/decline rates, and short-lived features. Hiramatsu et al. (2024) measured light curves of a large SNe IIn sample; they find a tight correlation between rise/decline times and peak magnitude and identify two subgroups of luminous-slow and faint-fast events. They suspect that the luminous-slow subgroup likely originates from more massive progenitors while the faint-fast subgroup may correspond to explosions of less massive progenitors. In parallel, Ransome & Villar (2025) applies light curve fitting of ejecta-CSM interaction models and reports that SNe IIn with more massive CSM have longer r -band rise/decline times and brighter peak magnitudes (see also Nyholm et al. 2020). Therefore it seems that the peak magnitudes of SNe IIn can serve as a useful proxy of CSM properties. Moreover, the measurement of peak magnitudes is much easier than that of other SNe observables (such as the rise/decline time, which requires good sampling of the light curve, but in our sample such light curves are always not available). In the following subsections, we try to investigate the relation between the peak magnitude and the local environment of SNe IIn.

We collected the peak magnitudes for the SNe in our sample and applied the reported host extinctions from the literature. These values, along with corresponding references, are summarized in Table 1. For 25 SNe, we preferentially used r/R /unfiltered (unf)-band photometry near the peak. For the 6 objects lacking r/R /unfiltered (unf)-band photometry, we used

$B/V/I$ -band photometry instead, which are very close to r/R /unfiltered (unf)-band photometry as optical colors at the SN peak are close to zero (de Jaeger et al. 2019). For 10 SNe without photometric observations near the maximum luminosity, we adopted the brightest available measurement as a lower limit of the peak magnitude. In the case of SN 2009ip-like objects showing double peaks, we adopted the brighter peak of the second event. With the respective distances applied and corrections made for both Galactic (Schlafly & Finkbeiner 2011) and host extinction (from the literature), we plot the resulting peak absolute magnitudes (M_{peak}) against the SNe environment classes in Figure 4. Within each environment class, the SNe are ordered by their M_{peak} and labelled accordingly.

4.1. “Bright” SNe IIn

As shown in Figure 4, the SNe IIn in our sample exhibit clear separations in peak magnitude. Five objects with $M_{\text{peak}} < -19.5$ mag are notably more luminous than the rest. We designate them as the “Bright” SNe IIn, and some have even been designated as superluminous SNe IIn in literature. Such high luminosities are commonly explained by extreme CSM interaction in iron core-collapse SNe or pair-instability SNe (Woosley et al. 2007; Smith et al. 2007), in which a substantial fraction of ejecta kinetic energy is dissipated and efficiently converted to optical radiation (van Marle et al. 2010; Suzuki et al. 2020). To power these bright transients, the CSM mass is estimated to be least 5–10 M_{\odot} , and in some cases as high as 20–40 M_{\odot} (Smith et al. 2008; Nicholl et al. 2020), that, in turn, implies very massive progenitors.

An alternative model for such luminous event invokes thermonuclear explosions of white dwarfs in binary systems following a common-envelope phase shortly before the Type Ia SNe (Ablimit 2021), normally named as Type Ia-CSM (Hamuy et al. 2003; Silverman et al. 2013). Leloudas et al. (2015) demonstrated that strong CSM interaction can mask an underlying SN Ia spectrum, and such Ia-CSM events typically exhibit a bright absolute magnitude range $-19.5 > M > -21.6$, overlapping the luminosities of our ‘Bright’ SNe IIn. In this scenario, the progenitor is a low-mass star. The well-studied “Bright” Type IIn SN 2006gy exemplifies the ongoing debate over the progenitor identity (Jerkstrand et al. 2020).

Insights of progenitor masses could be inferred from environmental analysis. We find that four of the five “Bright” SNe IIn in our sample located in the Class 1 environment, which are likely associated with very massive progenitors. In previous works, we have performed detailed modelling of stellar populations in vicinity of

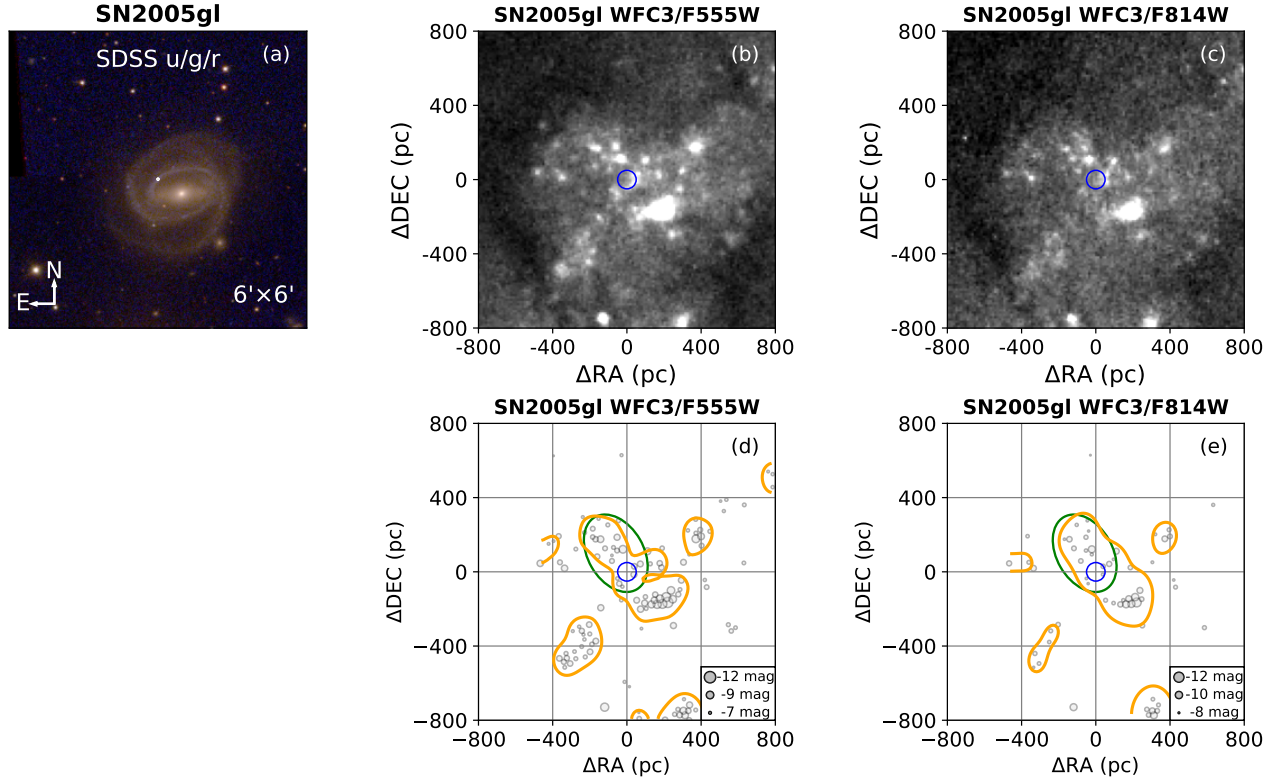


Figure 1. The environment of SN 2005gl serves as an example of a Class 1 environment, located within a star-forming region. (a) SDSS $u/g/r$ composite image of the host galaxy, centered on the SN. The white square outlines an 800 pc \times 800 pc zoomed-in region. (b, c) HST images of the SN site. (d, e) Spatial distribution of stars detected in the HST images. Symbol sizes represent absolute magnitudes corrected for Galactic extinction. The orange contour traces a 3σ density enhancement above the local average. Blue circles in panels (b–e) indicate a 50 pc radius centered on the derived SN site, considering the positional uncertainties of the SN in Section 2.3. The green elongated circle in panel (d) outlines the nearest stellar overdensity region to the SN, which is spatially distinct from the dense region southeast of the SN. Stars within this circle are considered to be coeval with the SN progenitor and are used for comparison in analysis in Section 5.

SN 2010jl and found that it likely originated from a very young environment with very recent star formation (Niu et al. 2024). Similarly, Ofek et al. (2007) and Brennan et al. (2024) also report star-forming environments for the “Bright” Type IIn SNe 2006gy and 2021adxl, respectively. While there are no obvious resolved stellar populations near the SN 2017hcc, its environment classification might be affected by the bright SN itself and the shallow detection limit in the UV band, and we can not rule out an underlying star-forming region at the SN position. Therefore, the “Bright” SNe IIn are most likely to originate from very massive progenitors.

4.2. “Normal” SNe IIn

The majority of SNe IIn share a typical peak magnitude in the range of $-19.5 < M_{\text{peak}} < -15.5$ mag and are denoted as “Normal” SNe IIn (e.g., Richardson et al. 2014; Pessi et al. 2025). For their pre-SN mass loss, observational evidences suggest high rate of $\geq 10^{-3} M_{\odot} \text{ yr}^{-1}$ (e.g. Kiewe et al. 2012; Moriya et al. 2014). The associated CSM is estimated to have a mass range of $0.5\text{--}8 M_{\odot}$, extending to radii of tens of AU (e.g., Ransom & Villar 2025). Interestingly, these “Normal” SNe IIn are observed across all three environment classes. This diversity suggests a wide range of progenitor population ages and initial masses. This indicates that their CSM properties are insensitive to the initial mass, or that the final CSM results from multiple physical mechanisms.

Several processes have been investigated. For example steady wind mass loss, which is closely tied to stellar mass (Lamers & Cassinelli 1999), and for evolved stars the mass loss rates are typically in the range of $10^{-6}\text{--}10^{-3} M_{\odot} \text{ yr}^{-1}$ (Smith 2017), which is not compatible to the observed value inferred for SNe IIn. Other processes have been invoked to account for this discrepancy. Episodic mass loss can be triggered by pulsations (Yoon & Cantiello 2010), S Doradus-type instabilities (Levesque et al. 2025), or wave-heating energy depositions (Quataert & Shiode 2012; Shiode & Quataert 2014). Through pulsations and S Doradus-type instabilities, mass loss rates are generally on the order of $\leq 10^{-4} M_{\odot} \text{ yr}^{-1}$. For the wave-heating mechanism, its efficiency remains controversial (Wu & Fuller 2021; Leung et al. 2021) that the main outcome may be inflating stellar envelope rather than substantial mass ejection (Mcley & Soker 2014; Fuller 2017; Wu & Fuller 2022). Binary interaction has been widely proposed as a viable channel for violent eruptions (Smith & Arnett 2014; Schrøder et al. 2020; Ercolino et al. 2024), and the directly detected LBVs progenitors could form via binary merger and/or mass accretion (Justham et al. 2014;

Smith & Tombleson 2015; Hirai et al. 2021). In addition, spectropolarimetric observations have revealed persistent CSM asymmetry in many SNe IIn (Wang et al. 2001; Mauerhan et al. 2014; Bilinski et al. 2018, 2024), which is most naturally explained by the interacting binaries.

4.3. “Faint” SNe IIn

Three SNe IIn in our sample exhibit peak magnitudes fainter than $M_{\text{peak}} < -15.5$ mag, approaching the lower luminosity limit of core-collapse SNe. Two of them (SNe 1978K and 1996bu) were not observed at the peak light, yet their lower limits of peak brightness are ~ 2.5 mag fainter than the faintest among “Normal” SNe IIn, justifying their classification as “Faint”. Their inferred pre-SN mass loss rates are $10^{-4}\text{--}10^{-3} M_{\odot} \text{ yr}^{-1}$ (Ryder et al. 1993; Chugai et al. 1995; Kochanek et al. 2012; Chiba et al. 2020; Adams & Kochanek 2015), lower than those of “Bright” and “Normal” SNe IIn.

At such faint magnitudes, the population overlaps with non-terminal SN impostors (e.g., outbursts of η Carinae and P Cygni, Smith et al. 2011a; Smith & Frew 2011). This raises a question of whether the “Faint” SNe IIn represent genuine terminal explosions or the brightest members of the impostor population. In particular, SN 1997bs has long been considered as an SN impostor (Van Dyk et al. 2000; Smith et al. 2011a; Kochanek et al. 2012). If this interpretation holds, the “Faint” SNe IIn should be exclusively observed in Classes 1 and 2. However, this contradicts our findings that all “Faint” objects are associated with Classes 2 and 3, passively star-forming environments. This environmental trend suggests that the “Faint” SNe IIn likely correspond to much lower massive progenitors.

The environments of “Faint” SNe IIn support an alternative scenario that they were genuine but subluminous SNe IIn resulting from weak explosions ($< 10^{51}$ erg) of stars with masses of $8\text{--}10 M_{\odot}$. In such SNe, very little ^{56}Ni ($\sim 10^{-3} M_{\odot}$) was synthesized, and conversion from shock energy to radiation energy through CSM interaction is not very efficient. This scenario is also supported by the observed low ejecta velocities (Van Dyk et al. 2000; Smith & Frew 2011; Davidson & Humphreys 2012; Ryder et al. 1993). Moreover, Adams & Kochanek (2015) points out that type “Faint” Type IIn SN 1997bs has continued to fade in optical and infrared bands and remains significantly fainter than its progenitor star, a behavior they argue is consistent with a terminal supernova explosion. It should be noted that the “Faint” SNe IIn discussed here are still considerably brighter than many known SN impostors (peak magnitudes of about -10 mag; Maund et al. 2006; Smith et al. 2011a).

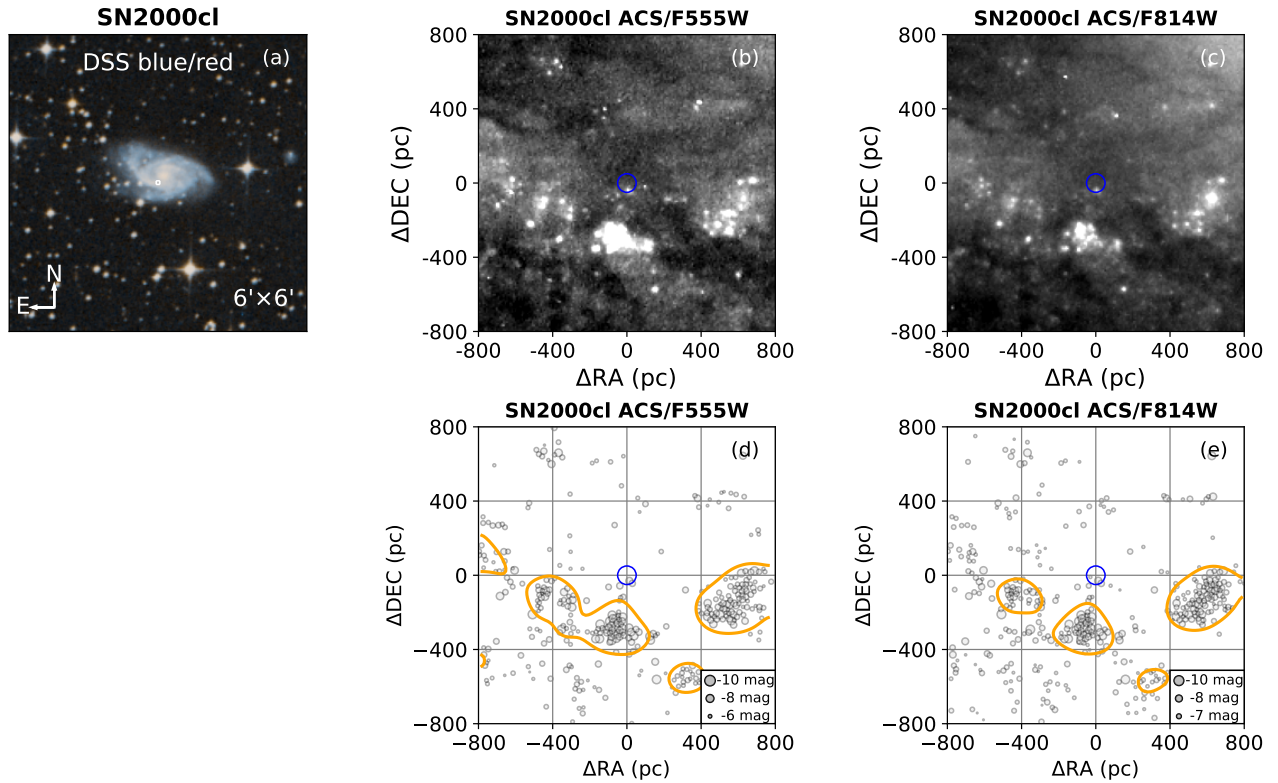


Figure 2. Similar to Figure 1, but for SN 2000cl. No stellar overdensity is detected within 50 pc of the SN; however, a significant overdensity of stars is detected within 300 pc. This distance approximately corresponds to the spatial displacement within which 90% of progenitors that have undergone binary interactions. (Wagg et al. 2025; Renzo et al. 2019). Therefore, environments such as that of SN 2000cl are defined as Class 2, indicating locations outside star-forming regions.

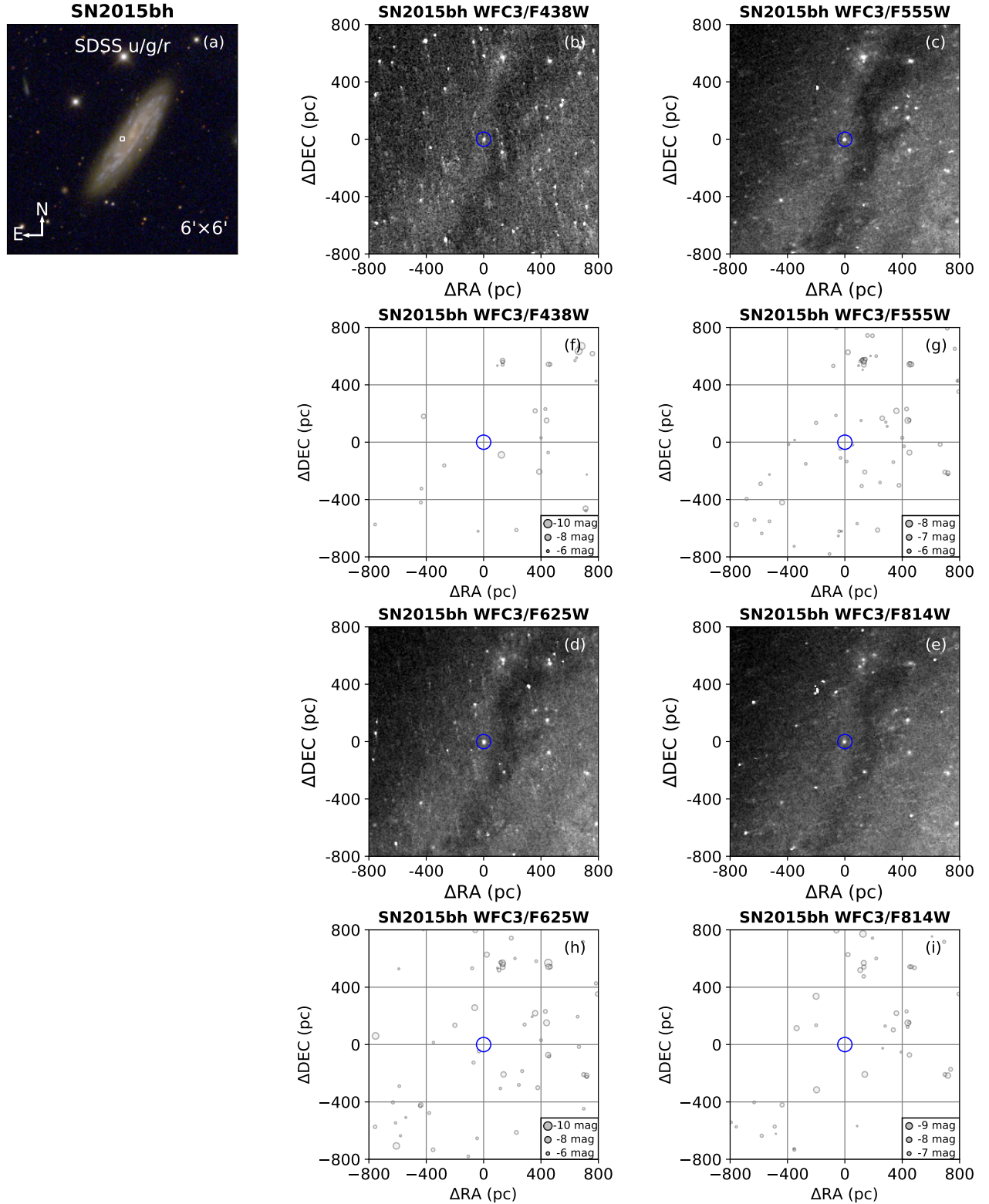


Figure 3. Similar to Figures 1 and 2, but for SN 2015bh. This environment lacks strong evidence for star-forming regions within 300 pc and is therefore defined as Class 3.

Environmental studies of such fainter impostors can be found in [Habergham et al. \(2014\)](#).

4.4. Significance of the Environment–Luminosity Correlation

To assess the statistical significance of the observed correlation between SN luminosity and environmental class, we performed Fisher exact tests for the association of “Bright”/“Faint” vs. Class 1/non-Class 1 environments. Given that the environmental Class of two bright SN (SN 2017hcc and Gaia14ahl) remains uncertain (see Section 3), we conducted a sensitivity analysis under three scenarios: (1) both are assigned to Class 1; (2) one belongs to Class 1 and the other belongs to non-Class 1; (3) both are assigned to non-Class 1. The corresponding p values for these scenarios are 0.0048, 0.0048, and 0.214, respectively. The association is statistically significant ($p < 0.05$) under the first two scenarios, which we consider the most realistic given the potential observational limitations (e.g., obscuration by the SN itself or shallow UV imaging depth). Only under the most conservative case, the correlation fail to meet the conventional significance threshold.

The observed absence of “Faint” SNe IIn in Class 1 is unlikely because of the observational bias. SNe are usually discovered through image subtraction techniques, which are sensitive to detecting faint transients even in bright regions such as star-forming complexes. This view is supported by [Senzel et al. \(2025\)](#), which shows that the fainter SNe Ia are actually more frequent in regions with higher surface brightness. Thus, the exclusive association of “Faint” SNe IIn with older stellar populations appears robust.

Our results align with the environmental trends reported by [Moriya et al. \(2023\)](#), who found that SNe IIn with higher peak luminosities tend to occur in environments with lower metallicity and/or younger stellar populations, with correlation coefficients of approximately $p = 0.6 \pm 0.1$ and $p = 0.4 \pm 0.1$, respectively. In particular, their results reinforce our conclusion for the “Bright” SNe IIn; their brightest SNe IIn of $M \leq -19$ (corresponding to our “Bright” subsample) are clearly associated with younger stellar populations, while within their normal-luminous SNe IIn ($M \geq -19$), no strong trend is found between peak magnitude and stellar population age or metallicity. The agreement between our independent samples and methodologies strengthens the robustness of the emerging picture regarding the diversity of SNe IIn progenitors and the interpretation that “Bright” SNe IIn are statistically linked to young star-forming regions (Class 1), while “Faint” SNe IIn exclusively arise in older, non-star-forming environments (Classes 2 and 3).

We further note that the sample of [Moriya et al. \(2023\)](#) does not include counterparts to our “Faint” SNe IIn; our work therefore extends the environmental mapping of SNe IIn to lower luminosities by revealing their exclusive association with much older stellar environments.

Our reclassification for the environmental Class for a few SNe could, in principle, work for other SNe IIn in our sample. For example, some sparse environments might host undetected star-forming regions due to dust extinction or insufficient imaging depth. Nevertheless, such potential biases would not alter our main conclusions: (1) For the “Bright” SNe IIn, we have considered the potential influence on the statistical significant above, and the luminosity-environment pattern is further supported by the independent findings of [Moriya et al. \(2023\)](#); (2) For the “Normal” SNe IIn, our main conclusion is the diversity across all three environments. This result is not sensitive to the possible presence of a few undetected star-forming regions; (3) For the “Faint” SNe IIn, the three defining objects are among the photometrically best-observed in our sample (see Appendix C), making their exclusive link to Class 3 environments the least likely to be affected by detection limits. While future deeper, multi-wavelength observations may refine the environmental census, the luminosity-environment correlation and the diversity of environments reported in this work are robust against the potential biases discussed here.

5. COMPARISON WITH DIRECT PROGENITOR DETECTIONS

Among the analyzed SNe IIn, we have a subsample in which their progenitors have been directly detected. The subsample comprises SNe 1997bs ([Van Dyk et al. 1999, 2000](#)), 2005gl ([Gal-Yam et al. 2007; Gal-Yam & Leonard 2009](#)), 2009ip ([Smith et al. 2010; Foley et al. 2011; Ofek et al. 2013](#)), 2010bt ([Elias-Rosa et al. 2018](#)), 2010jl ([Smith et al. 2011b; Fox et al. 2017; Niu et al. 2024](#)), 2015bh ([Elias-Rosa et al. 2016; Thöne et al. 2017; Boian & Groh 2018](#)) and 2016jbu ([Kilpatrick et al. 2018; Brennan et al. 2022b](#)). These SNe have been extensively observed and studied after their explosions; their host extinctions and metallicities at SNe sites have been well determined. We take these advantages to analysis the relationship between the progenitors and their surrounding stellar populations.

Figure 5 presents the color-absolute magnitude diagram (CMD) for SNe progenitors and resolved point sources around them that are detected in both photometric bands. The reported progenitors of SNe 2010jl, 2015bh, and 2016jbu were detected in multiple bands, including bands that are used for environmental analysis

Table 1. Metallicity, distance, peak magnitude, host extinction, and environment class for the SN IIn sample in this work.

Name	12+log([O/H]) dex	Distance Mpc	M_{peak}^{**} mag	A_{host} mag	Class
SN1961V	8.77 ^a	9.3	12.70(0.00) ^b	-	1
SN1994W	8.61 ^c	16.9	13.30(0.00) ^d	0.37 ^c	1
SN1997eg	8.53 ^e	35.6	<15.27 ^f	-	1
SN2005gl	8.59 ^c	63.4	17.00(0.10) ^{†,c}	0.09 ^g	1
SN2005ip	8.93 ^a	29.5	<15.04 ^c	-	1
SN2006gy	8.70 ^h	78.8	14.22(0.03) ⁱ	1.40 ^{i,h}	1
SN2009ip	8.25 ^j	24.1	13.65(0.10) ^{†,c}	0.03 ^k	1 [*]
SN2010jj	-	70.6	<16.22 ^l	-	1
SN2010jl	8.25 ^m	43.8	13.00(0.10) ^m	0.06 ^k	1
SN2010jp	8.54 ⁿ	37.7	17.20(0.00) ^o	$\approx 0^p$	1 [*]
SN2013gc	-	13.9	14.66(0.14) ^{†,q}	$\approx 0^q$	1
Gaia14ahl	-	69.7	14.17(0.00) ^k	0.07 ^k	1 [*]
SN2015bf	8.49 ^r	58.3	15.66(0.05) ^s	0.19 ^s	1 [*]
SN2016jbu	8.56 ^r	19.6	13.80(0.05) ^{†,t}	$\approx 0^u$	1
SN2019njv	-	59.8	18.08(0.06) ^v	-	1
SN2021adxl	7.61 ^w	73.8	14.32(0.02) ^w	$\approx 0^w$	1
SN1978G	8.19 ^r	12.7	<12.90 ^b	-	2
SN1978K	8.07 ^x	4.61	<16.00 ^y	0.23 ^z	2
SN1997bs	8.59 ^r	9.4	16.83(0.03) ^{aa}	$\approx 0^{aa}$	2
SN1998S	8.67 ^c	12.3	12.19(0.00) ^c	0.43 ^{bb}	2
SN1999el	8.17 ^e	19.2	14.52(0.04) ^{cc}	0.47 ^{cc}	2
SN2000c1	8.53 ^r	37.7	<14.80 ^{dd}	-	2
SN2008fq	8.58 ^r	43.5	15.40(0.00) ^{ee}	0.99 ^{ff}	2
SN2011ht	8.20 ^{gg}	14.7	14.15(0.09) ^c	0.06 ^k	2
SN1996bu	-	16.0	<17.60 ^{hh}	-	3
SN1994Y	8.74 ⁱⁱ	34.8	14.20(0.02) ^{jj}	$\approx 0^c$	3
SN2003lo	8.61 ^c	57.4	<17.20 ^c	-	3
SN2010bt	8.61 ^r	66.3	<16.00 ^{kk}	0.80 ^{kk}	3
SN2014es	-	80.4	<16.00 ^{ll}	-	3 [*]
SN2015bh	8.46 ^{mm}	26.2	15.35(0.07) ^{†,nn}	0.15 ^k	3
SN2017hcc	8.49 ^{oo}	71.0	12.46(0.06) ^{oo}	0.03 ^k	3 [*]

^{*}: Preliminary classification of the SN environment.^{**}: The peak magnitudes have been corrected for Galactic extinction based on the SFD extinction map (Schlafly & Finkbeiner 2011). Peak magnitudes for SN 1978K (*B*), SNe 2010jl and 2013gc (*I*), and SNe 1978G, 1996bu, 1994W (*V*) were obtained in the specified bands; the remaining SNe were observed in *R*, *r*, or unfiltered bands.[†]: SN 2009ip-like, taking the peak magnitude of the second event.

References: a: Xiao et al. (2019), b: Barbon et al. (1999), c: Taddia et al. (2015), d: Sollerman et al. (1998), e: Habergham et al. (2014), f: Tsvetkov & Pavlyuk (2004), g: Gal-Yam et al. (2007), h: Ofek et al. (2007), i: Smith et al. (2007), j: Margutti et al. (2014), k: Bilinski et al. (2024), l: Ofek et al. (2014), m: Stoll et al. (2011), n: Corgan et al. (2022), o: Maza et al. (2010), p: Smith et al. (2012), q: Reguitti et al. (2019), r: Xi et al. (2025), s: Lin et al. (2021), t: Brennan et al. (2022a), u: Brennan et al. (2022b), v: ZTF, w: Brennan et al. (2024), x: Chiba et al. (2020), y: Ryder et al. (1993), z: Chugai et al. (1995), aa: Van Dyk et al. (2000), bb: Fassia et al. (2000), cc: Di Carlo et al. (2002), dd: Stathakis & Stevenson (2001), ee: Bilinski et al. (2015), ff: Taddia et al. (2013), gg: Roming et al. (2012), hh: Armstrong & Hurst (1996), ii: Kelly & Kirshner (2012), jj: Ho et al. (2001), kk: Elias-Rosa et al. (2018), ll: Li et al. (2014), mm: Thöne et al. (2017), nn: de la Rosa et al. (2016), oo: Moran et al. (2023)

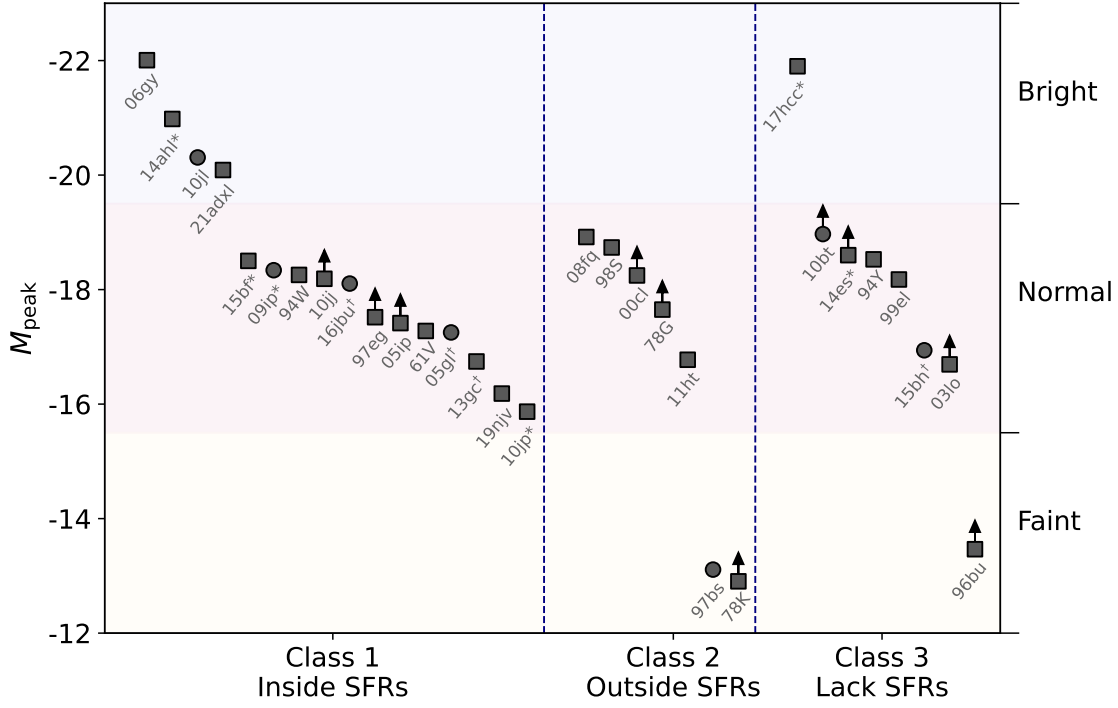


Figure 4. Peak absolute magnitude versus local environment class for 31 SNe IIn at $z < 0.02$ with HST high-resolution imaging. The local environments of SNe are classified into three types based on resolved stellar populations: inside star-forming regions, outside star-forming regions, or regions lacking obvious star-forming regions. Those SNe for which the classification of their host environment is still preliminary are indicated with *. Following the SNe IIn light curve census of [Ransome & Villar \(2025\)](#), we classify their peak absolute magnitudes as: bright ($M_{\text{peak}} < -20$), normal ($-20 < M_{\text{peak}} < -16$), or faint ($M_{\text{peak}} > -16$). The 2009ip-like SNe (showing two luminous peaks) are marked with †. SNe whose progenitors have been directly detected are indicated with circles; their progenitors and environmental stars are analyzed in detail in Section 5.

in this work. The progenitor of SN 2010bt was detected in ACS/F330W band in 2003 and WFPC2/F606W band in 1994; due to a 9-years difference and the common occurrence of variability in possible progenitors, only the F606W-band magnitude is plotted as a horizontal line, with width representing 1σ uncertainty. Similarly, SN 2009ip's progenitor was only observed in WFPC3/F606W band prior to the explosion and is also indicated by a horizontal line. The progenitors of SNe 1997bs (WFPC2/F606W) and 2005gl (WFPC2/F547M) were observed in bands differing from those for the environmental analysis. We interpolate progenitor magnitudes to the CMD bands using a blackbody SED with effective temperatures spanning $10^{3.3}\text{--}10^{5.0}$ K and plot them in stripes.

These seven SNe IIn cover all environment classes. SNe 2005gl, 2010jl, and 2016jbu are considered to be the Class 1 objects, and we plot resolved stars within their likely birth star-forming regions. We have reclassified SN 2009ip as Class 1 based on the discussion above; however, only one source is detected within 300 pc to the southeast of SN 2009ip. This point source has been studied in detail by Smith et al. (2016). PARSEC (Bresan et al. 2012; Chen et al. 2014, 2015; Tang et al. 2014) single-star isochrones of various initial masses are overlaid for references. Clearly, their progenitors are brighter and/or bluer than the youngest stellar populations in the SNe environment, regardless of whether the local stellar ages are extremely young, $M_{\text{ini}} \approx 50 M_{\odot}$ for SNe 2005gl and 2010jl, or moderately young, $M_{\text{ini}} \approx 20 M_{\odot}$ for SN 2016jbu.

SNe 1997bs belongs to the Class 2. Since it was outside but close to the stellar overdensity, we considered stars within 300 pc of the SN, and we supposed that stars outside the enhancements represent uniform background populations corresponding to the oldest stellar component. We identified the background (BKG) members within the enhanced regions by matching photometric counterparts (within 1σ color and magnitude uncertainties) from the outside population. The remaining members are considered to be from the star-forming (SF) populations, representing younger stellar populations. In Figure 5, the SF and BKG populations are plotted in orange and gray, respectively. The SF population in the vicinity exhibits $M_{\text{ini}} > 10 M_{\odot}$, contrasting with the lower-mass ($M_{\text{ini}} < 10 M_{\odot}$) BKG population. We note that the progenitor is anomalous among SNe IIn. This peculiar faintness may be physically linked to the low SN luminosity as we discussed in Section 4.3. If the progenitor belonged to the BKG population, its high brightness would align with relationships observed for other Type IIn progenitors and their sur-

rounding stars; alternatively, the progenitor could be fitted with single-star isochrones of $\sim 20\text{--}30 M_{\odot}$.

SNe 2010bt and 2015bh were assigned Class 3, being located in a very sparse environment, lacking obvious star-forming activity. Stars in the vicinity of SN 2015bh are not as young as that of Class 1 and 2, with the youngest population less massive than $20 M_{\odot}$. The resolved sources surrounding SN 2010bt are all extremely young, likely a consequence of the short exposure times that results in detections of only the brightest, most massive stars. Even with this limitation, the progenitor remained at least 1 mag brighter than all neighboring sources in the F606W band.

We conclude that Type IIn SNe progenitors stand out from their local stellar populations in terms of magnitude and/or color. This provides strong evidence that their progenitors are in a non-quiescent state and/or have experienced binary interactions (i.e. mergers or mass accretion) prior to explosion. In fact, mergers have been suggested to contribute significantly to the diversity of SNe, including SNe IIn (Justham et al. 2014; Zapartas et al. 2019; Schneider et al. 2024). The tension in initial mass/ages between the detected SNe progenitors and the stars in their environments has been used to identify the interacting binary histories of H-rich SNe (Zapartas et al. 2021; Bostroem et al. 2023, Niu et.al. in prep.). Therefore, the stellar parameters, particularly the initial mass and age, of SNe IIn progenitors cannot be reliably estimated by standard single-star models. Meanwhile, combined with the result from Section 4, our number-limited subsample also suggests that SNe IIn may originate from stellar populations with wide mass, not exclusively from very massive stellar populations, but potentially from populations with initial masses as low as $M_{\text{ini}} < 20 M_{\odot}$.

6. SUMMARY

In this paper, we present a study of the local environments of 31 SNe IIn within a volume-limited sample ($z < 0.02$), utilizing high-resolution archival imaging from the HST. Their environments are diverse, and we classified them into three categories: Class 1, where the SN located within active star-forming regions; Class 2, where the SN was outside but close to star-forming regions; and Class 3, where no significant star-forming region is detected around the SN. These reveal a significant diversity of SNe IIn environments, suggesting that SNe IIn progenitors should have multiple evolutionary pathway with a range of initial masses and lifetimes.

Our investigation reveals a clear correlation between peak absolute magnitudes of SNe IIn and their local environments. The “Bright” SNe IIn, with $M_{\text{peak}} < -19.5$

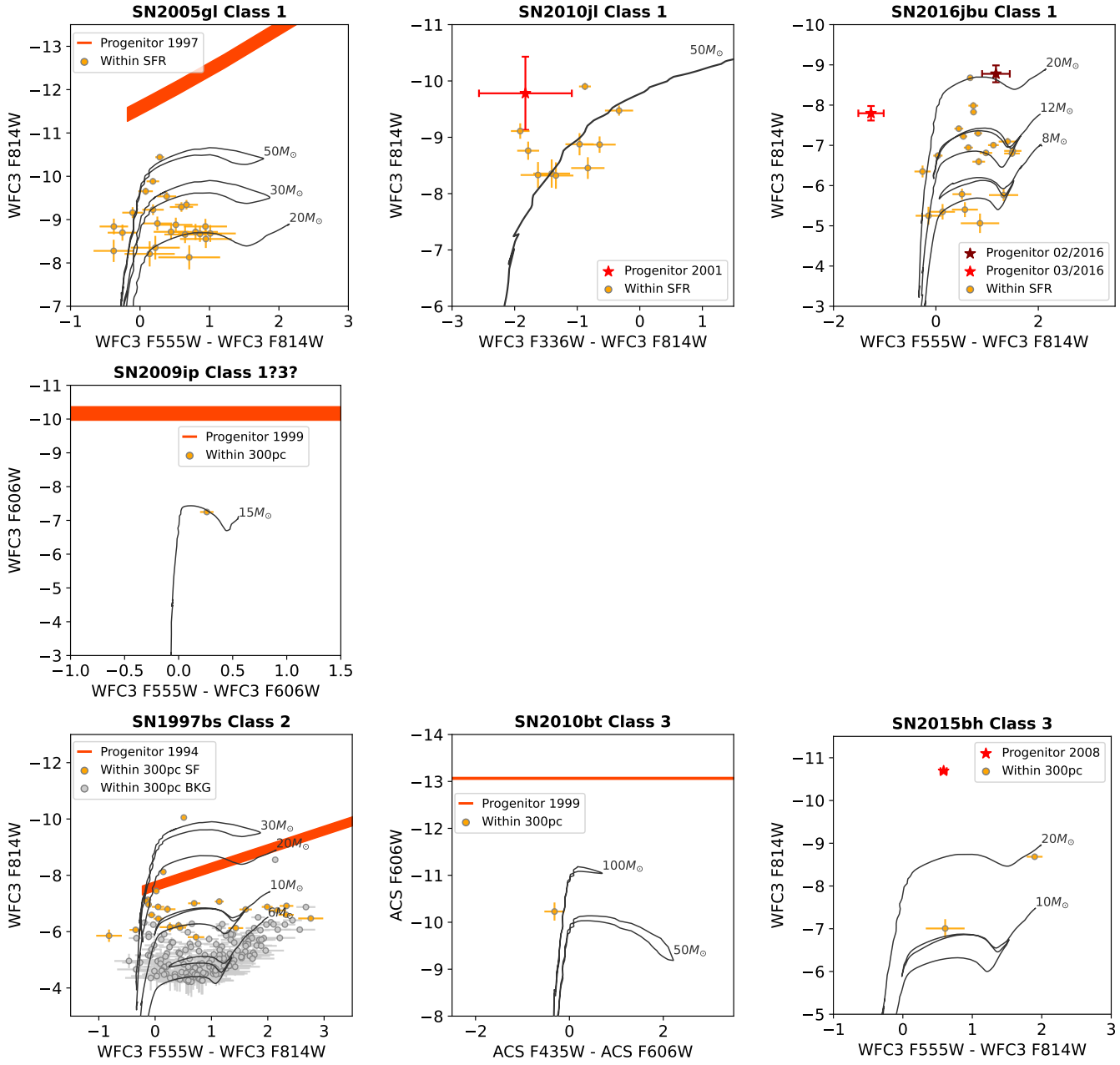


Figure 5. Color-absolute magnitude diagrams of the resolved stellar populations surrounding the site of seven SNe IIn with progenitor detections. Each panel is labeled with the SN name and its environmental Class. The directly detected progenitors are marked in red, with asterisks for well-constrained detections and horizontal stripes for less certain ones. For Class 1, the progenitors are compared to stars in the nearest star-forming region. For Class 2, we plot stars within 300 pc of the SN site. The star-forming population is shown in orange, and the background population is shown in gray (see text). The Class 3 environments lack obvious star-forming regions, therefore surrounding stars within 300 pc are shown. The classification of SN 2009ip is uncertain (see discussion in the text). The only point source detected within 300 pc of its position has been studied in detail by [Smith et al. \(2016\)](#). Corrections have been applied for both Galactic extinction (SFD map) and host extinction (in literature) for the progenitor and surrounding stellar. The widths of stripes and errorbars represent 1σ uncertainties. PARSEC single-star isochrones, with labelled initial masses, are overlaid.

mag, are overwhelmingly found in Class 1 environments, suggesting that they originate from very massive progenitors. The “Faint” SNe IIn in our sample, with $M_{\text{peak}} > -15.5$, are exclusively associated with older, non-star-forming environments (Classes 2 and 3), indicating that such events are likely genuine SN explosions from the lowest-mass massive progenitors rather than giant eruptions of very massive stars. Meanwhile, the “Normal” SNe IIn, with $-19.5 < M_{\text{peak}} < -15.5$ mag, are found across all three environment classes. This diversity implies that their progenitors have different initial masses and their pre-SN mass loss could be mass-insensitive and/or due to multiple physical processes.

For seven SNe IIn with direct progenitor detections in pre-explosion images, we compared the progenitors to their resolved surrounding stellar populations. These progenitors are consistently more luminous and/or bluer than the youngest population in their vicinity. This provides observational evidence that they were either in a non-quiescent state or have experienced binary merger/gainer prior to explosion. Consequently, their physical properties cannot be reliably interpreted using

standard single-star evolutionary models. Again, this is against the transitional view that SNe IIn are exclusively from very massive stars. The inferred stellar populations have a wide range of initial masses, potentially extending down to $M_{\text{ini}} < 20M_{\odot}$.

We note that the present sample, while valuable, is inherently limited by the availability of HST archival data and our current sample represents only a fraction of the known SNe IIn population. This limitation currently prevents a sophisticated statistical investigation into the potential environmental dependencies of various proposed sub-types of SNe IIn, such as the IIn-P, the 1998S-like, the 2009ip-like events. The environment-based approach established in this work provides a clear framework for future studies. We anticipate that a significant expansion of the sample, leveraging future high-resolution, wide-field, and multi-wavelength (particularly in the infrared) data from observatories such as the Vera C. Rubin Observatory’s Legacy Survey of Space and Time (LSST), the China Space Station Survey Telescope (CSST), and the James Webb Space Telescope (JWST) will be transformative.

REFERENCES

Ablimit, I. 2021, PASP, 133, 074201, doi: [10.1088/1538-3873/ac025c](https://doi.org/10.1088/1538-3873/ac025c)

Adams, S. M., & Kochanek, C. S. 2015, MNRAS, 452, 2195, doi: [10.1093/mnras/stv1409](https://doi.org/10.1093/mnras/stv1409)

Anderson, J. P., Habergham, S. M., James, P. A., & Hamuy, M. 2012, MNRAS, 424, 1372, doi: [10.1111/j.1365-2966.2012.21324.x](https://doi.org/10.1111/j.1365-2966.2012.21324.x)

Anderson, J. P., & James, P. A. 2008, MNRAS, 390, 1527, doi: [10.1111/j.1365-2966.2008.13843.x](https://doi.org/10.1111/j.1365-2966.2008.13843.x)

Armstrong, M., & Hurst, G. M. 1996, IAUC, 6509, 2

Barbon, R., Buondí, V., Cappellaro, E., & Turatto, M. 1999, A&AS, 139, 531, doi: [10.1051/aas:1999404](https://doi.org/10.1051/aas:1999404)

Berger, E., Soderberg, A. M., Chevalier, R. A., et al. 2009, ApJ, 699, 1850, doi: [10.1088/0004-637X/699/2/1850](https://doi.org/10.1088/0004-637X/699/2/1850)

Bilinski, C., Smith, N., Li, W., et al. 2015, MNRAS, 450, 246, doi: [10.1093/mnras/stv566](https://doi.org/10.1093/mnras/stv566)

Bilinski, C., Smith, N., Williams, G. G., et al. 2024, MNRAS, 529, 1104, doi: [10.1093/mnras/stae380](https://doi.org/10.1093/mnras/stae380)

—. 2018, MNRAS, 475, 1104, doi: [10.1093/mnras/stx3214](https://doi.org/10.1093/mnras/stx3214)

Boian, I., & Groh, J. H. 2018, A&A, 617, A115, doi: [10.1051/0004-6361/201731794](https://doi.org/10.1051/0004-6361/201731794)

Bostroem, K. A., Zapartas, E., Koplitz, B., et al. 2023, AJ, 166, 255, doi: [10.3847/1538-3881/acffc7](https://doi.org/10.3847/1538-3881/acffc7)

Brennan, S. J., Fraser, M., Johansson, J., et al. 2022a, MNRAS, 513, 5642, doi: [10.1093/mnras/stac1243](https://doi.org/10.1093/mnras/stac1243)

—. 2022b, MNRAS, 513, 5666, doi: [10.1093/mnras/stac1228](https://doi.org/10.1093/mnras/stac1228)

Brennan, S. J., Schulze, S., Lunnan, R., et al. 2024, A&A, 690, A259, doi: [10.1051/0004-6361/202349036](https://doi.org/10.1051/0004-6361/202349036)

Bressan, A., Marigo, P., Girardi, L., et al. 2012, MNRAS, 427, 127, doi: [10.1111/j.1365-2966.2012.21948.x](https://doi.org/10.1111/j.1365-2966.2012.21948.x)

Cai, Y.-Z., Pastorello, A., Fraser, M., et al. 2021, A&A, 654, A157, doi: [10.1051/0004-6361/202141078](https://doi.org/10.1051/0004-6361/202141078)

Chen, Y., Bressan, A., Girardi, L., et al. 2015, MNRAS, 452, 1068, doi: [10.1093/mnras/stv1281](https://doi.org/10.1093/mnras/stv1281)

Chen, Y., Girardi, L., Bressan, A., et al. 2014, MNRAS, 444, 2525, doi: [10.1093/mnras/stu1605](https://doi.org/10.1093/mnras/stu1605)

Cheng, S. J., Goldberg, J. A., Cantiello, M., et al. 2024, ApJ, 974, 270, doi: [10.3847/1538-4357/ad701e](https://doi.org/10.3847/1538-4357/ad701e)

Chiba, Y., Katsuda, S., Yoshida, T., Takahashi, K., & Umeda, H. 2020, PASJ, 72, 25, doi: [10.1093/pasj/psz148](https://doi.org/10.1093/pasj/psz148)

Chu, Y.-H., Gruendl, R. A., Stockdale, C. J., et al. 2004, AJ, 127, 2850, doi: [10.1086/383556](https://doi.org/10.1086/383556)

Chugai, N. N., Danziger, I. J., & della Valle, M. 1995, MNRAS, 276, 530, doi: [10.1093/mnras/276.2.530](https://doi.org/10.1093/mnras/276.2.530)

Conti, P. S., & Alschuler, W. R. 1971, ApJ, 170, 325, doi: [10.1086/151218](https://doi.org/10.1086/151218)

Corgan, A., Smith, N., Andrews, J., Filippenko, A. V., & Van Dyk, S. D. 2022, MNRAS, 510, 1, doi: [10.1093/mnras/stab2892](https://doi.org/10.1093/mnras/stab2892)

Davidson, K., & Humphreys, R. M., eds. 2012, *Astrophysics and Space Science Library*, Vol. 384, Eta Carinae and the Supernova Impostors, doi: [10.1007/978-1-4614-2275-4](https://doi.org/10.1007/978-1-4614-2275-4)

de Jaeger, T., Zheng, W., Stahl, B. E., et al. 2019, *MNRAS*, 490, 2799, doi: [10.1093/mnras/stz2714](https://doi.org/10.1093/mnras/stz2714)

de la Rosa, J., Roming, P., Pritchard, T., & Fryer, C. 2016, *ApJ*, 820, 74, doi: [10.3847/0004-637X/820/1/74](https://doi.org/10.3847/0004-637X/820/1/74)

Di Carlo, E., Massi, F., Valentini, G., et al. 2002, *ApJ*, 573, 144, doi: [10.1086/340496](https://doi.org/10.1086/340496)

Dolphin, A. 2016, DOLPHOT: Stellar photometry, *Astrophysics Source Code Library*, record ascl:1608.013. <http://ascl.net/1608.013>

Dolphin, A. E. 2000, *PASP*, 112, 1383, doi: [10.1086/316630](https://doi.org/10.1086/316630)

Elias-Rosa, N., Pastorello, A., Benetti, S., et al. 2016, *MNRAS*, 463, 3894, doi: [10.1093/mnras/stw2253](https://doi.org/10.1093/mnras/stw2253)

Elias-Rosa, N., Van Dyk, S. D., Benetti, S., et al. 2018, *ApJ*, 860, 68, doi: [10.3847/1538-4357/aac510](https://doi.org/10.3847/1538-4357/aac510)

Ercolino, A., Jin, H., Langer, N., & Dessart, L. 2024, *A&A*, 685, A58, doi: [10.1051/0004-6361/202347646](https://doi.org/10.1051/0004-6361/202347646)

Fassia, A., Meikle, W. P. S., Vacca, W. D., et al. 2000, *MNRAS*, 318, 1093, doi: [10.1046/j.1365-8711.2000.03797.x](https://doi.org/10.1046/j.1365-8711.2000.03797.x)

Foley, R. J., Berger, E., Fox, O., et al. 2011, *ApJ*, 732, 32, doi: [10.1088/0004-637X/732/1/32](https://doi.org/10.1088/0004-637X/732/1/32)

Fox, O. D., Smith, N., Ammons, S. M., et al. 2015, *MNRAS*, 454, 4366, doi: [10.1093/mnras/stv2270](https://doi.org/10.1093/mnras/stv2270)

Fox, O. D., Van Dyk, S. D., Dwek, E., et al. 2017, *ApJ*, 836, 222, doi: [10.3847/1538-4357/836/2/222](https://doi.org/10.3847/1538-4357/836/2/222)

Fox, O. D., Fransson, C., Smith, N., et al. 2020, *MNRAS*, 498, 517, doi: [10.1093/mnras/staa2324](https://doi.org/10.1093/mnras/staa2324)

Fuller, J. 2017, *MNRAS*, 470, 1642, doi: [10.1093/mnras/stx1314](https://doi.org/10.1093/mnras/stx1314)

Gal-Yam, A., & Leonard, D. C. 2009, *Nature*, 458, 865, doi: [10.1038/nature07934](https://doi.org/10.1038/nature07934)

Gal-Yam, A., Leonard, D. C., Fox, D. B., et al. 2007, *ApJ*, 656, 372, doi: [10.1086/510523](https://doi.org/10.1086/510523)

Galbany, L., Anderson, J. P., Sánchez, S. F., et al. 2018, *ApJ*, 855, 107, doi: [10.3847/1538-4357/aaaf20](https://doi.org/10.3847/1538-4357/aaaf20)

Garcia, L. J., Timmermans, M., Pozuelos, F. J., et al. 2022, *MNRAS*, 509, 4817, doi: [10.1093/mnras/stab3113](https://doi.org/10.1093/mnras/stab3113)

Gouliermis, D. A., Elmegreen, B. G., Elmegreen, D. M., et al. 2017, *MNRAS*, 468, 509, doi: [10.1093/mnras/stx445](https://doi.org/10.1093/mnras/stx445)

Habergham, S. M., Anderson, J. P., James, P. A., & Lyman, J. D. 2014, *MNRAS*, 441, 2230, doi: [10.1093/mnras/stu684](https://doi.org/10.1093/mnras/stu684)

Hamuy, M., Phillips, M. M., Suntzeff, N. B., et al. 2003, *Nature*, 424, 651, doi: [10.1038/nature01854](https://doi.org/10.1038/nature01854)

Heger, A., Fryer, C. L., Woosley, S. E., Langer, N., & Hartmann, D. H. 2003, *ApJ*, 591, 288, doi: [10.1086/375341](https://doi.org/10.1086/375341)

Hirai, R., Podsiadlowski, P., Owocki, S. P., Schneider, F. R. N., & Smith, N. 2021, *MNRAS*, 503, 4276, doi: [10.1093/mnras/stab571](https://doi.org/10.1093/mnras/stab571)

Hiramatsu, D., Berger, E., Gomez, S., et al. 2024, *arXiv e-prints*, arXiv:2411.07287, doi: [10.48550/arXiv.2411.07287](https://doi.org/10.48550/arXiv.2411.07287)

Ho, W. C. G., Van Dyk, S. D., Peng, C. Y., et al. 2001, *PASP*, 113, 1349, doi: [10.1086/323970](https://doi.org/10.1086/323970)

Humphreys, R. M., & Davidson, K. 1994, *PASP*, 106, 1025, doi: [10.1086/133478](https://doi.org/10.1086/133478)

Humphreys, R. M., Davidson, K., & Smith, N. 1999, *PASP*, 111, 1124, doi: [10.1086/316420](https://doi.org/10.1086/316420)

Jerkstrand, A., Maeda, K., & Kawabata, K. S. 2020, *Science*, 367, 415, doi: [10.1126/science.aaw1469](https://doi.org/10.1126/science.aaw1469)

Justham, S., Podsiadlowski, P., & Vink, J. S. 2014, *ApJ*, 796, 121, doi: [10.1088/0004-637X/796/2/121](https://doi.org/10.1088/0004-637X/796/2/121)

Kangas, T., Portinari, L., Mattila, S., et al. 2017, *A&A*, 597, A92, doi: [10.1051/0004-6361/201628705](https://doi.org/10.1051/0004-6361/201628705)

Kelly, P. L., & Kirshner, R. P. 2012, *ApJ*, 759, 107, doi: [10.1088/0004-637X/759/2/107](https://doi.org/10.1088/0004-637X/759/2/107)

Kiewe, M., Gal-Yam, A., Arcavi, I., et al. 2012, *ApJ*, 744, 10, doi: [10.1088/0004-637X/744/1/10](https://doi.org/10.1088/0004-637X/744/1/10)

Kilpatrick, C. D., Foley, R. J., Drout, M. R., et al. 2018, *MNRAS*, 473, 4805, doi: [10.1093/mnras/stx2675](https://doi.org/10.1093/mnras/stx2675)

Kochanek, C. S., Szczygiel, D. M., & Stanek, K. Z. 2011, *ApJ*, 737, 76, doi: [10.1088/0004-637X/737/2/76](https://doi.org/10.1088/0004-637X/737/2/76)

Kochanek, C. S., Szczygiel, D. M., & Stanek, K. Z. 2012, *ApJ*, 758, 142, doi: [10.1088/0004-637X/758/2/142](https://doi.org/10.1088/0004-637X/758/2/142)

Kroupa, P. 2002, *Science*, 295, 82, doi: [10.1126/science.1067524](https://doi.org/10.1126/science.1067524)

Kroupa, P., Weidner, C., Pflamm-Altenburg, J., et al. 2013, in *Planets, Stars and Stellar Systems. Volume 5: Galactic Structure and Stellar Populations*, ed. T. D. Oswalt & G. Gilmore, Vol. 5, 115, doi: [10.1007/978-94-007-5612-0_4](https://doi.org/10.1007/978-94-007-5612-0_4)

Lamers, H. J. G. L. M., & Cassinelli, J. P. 1999, *Introduction to Stellar Winds*

Lang, D., Hogg, D. W., Mierle, K., Blanton, M., & Rowels, S. 2010, *AJ*, 139, 1782, doi: [10.1088/0004-6256/139/5/1782](https://doi.org/10.1088/0004-6256/139/5/1782)

Leloudas, G., Hsiao, E. Y., Johansson, J., et al. 2015, *A&A*, 574, A61, doi: [10.1051/0004-6361/201322035](https://doi.org/10.1051/0004-6361/201322035)

Leung, S.-C., Wu, S., & Fuller, J. 2021, *ApJ*, 923, 41, doi: [10.3847/1538-4357/ac2c63](https://doi.org/10.3847/1538-4357/ac2c63)

Levesque, E. M., Lamers, H. J. G. L. M., & de Koter, A. 2025, *ApJ*, 981, 176, doi: [10.3847/1538-4357/adb581](https://doi.org/10.3847/1538-4357/adb581)

Li, W., Filippenko, A. V., Van Dyk, S. D., et al. 2002, *PASP*, 114, 403, doi: [10.1086/342493](https://doi.org/10.1086/342493)

Li, W., Wang, X., & Zhang, T. 2014, *The Astronomer's Telegram*, 6734, 1

Lin, H., Wang, X., Zhang, J., et al. 2021, MNRAS, 505, 4890, doi: [10.1093/mnras/stab1550](https://doi.org/10.1093/mnras/stab1550)

Margutti, R., Milisavljevic, D., Soderberg, A. M., et al. 2014, ApJ, 780, 21, doi: [10.1088/0004-637X/780/1/21](https://doi.org/10.1088/0004-637X/780/1/21)

Mauerhan, J., & Smith, N. 2012, MNRAS, 424, 2659, doi: [10.1111/j.1365-2966.2012.21325.x](https://doi.org/10.1111/j.1365-2966.2012.21325.x)

Mauerhan, J., Williams, G. G., Smith, N., et al. 2014, MNRAS, 442, 1166, doi: [10.1093/mnras/stu730](https://doi.org/10.1093/mnras/stu730)

Maund, J. R. 2018, MNRAS, 476, 2629, doi: [10.1093/mnras/sty093](https://doi.org/10.1093/mnras/sty093)

Maund, J. R., Smartt, S. J., Kudritzki, R.-P., et al. 2006, MNRAS, 369, 390, doi: [10.1111/j.1365-2966.2006.10308.x](https://doi.org/10.1111/j.1365-2966.2006.10308.x)

Maza, J., Hamuy, M., Antezana, R., et al. 2010, Central Bureau Electronic Telegrams, 2544, 1

Mcley, L., & Soker, N. 2014, MNRAS, 445, 2492, doi: [10.1093/mnras/stu1952](https://doi.org/10.1093/mnras/stu1952)

Moran, S., Fraser, M., Kotak, R., et al. 2023, A&A, 669, A51, doi: [10.1051/0004-6361/202244565](https://doi.org/10.1051/0004-6361/202244565)

Moriya, T. J., Maeda, K., Taddia, F., et al. 2014, MNRAS, 439, 2917, doi: [10.1093/mnras/stu163](https://doi.org/10.1093/mnras/stu163)

Moriya, T. J., Galbany, L., Jiménez-Palau, C., et al. 2023, A&A, 677, A20, doi: [10.1051/0004-6361/202346703](https://doi.org/10.1051/0004-6361/202346703)

Nicholl, M., Blanchard, P. K., Berger, E., et al. 2020, Nature Astronomy, 4, 893, doi: [10.1038/s41550-020-1066-7](https://doi.org/10.1038/s41550-020-1066-7)

Niu, Z., Sun, N.-C., & Liu, J. 2024, ApJL, 966, L20, doi: [10.3847/2041-8213/ad3f8f](https://doi.org/10.3847/2041-8213/ad3f8f)

Niu, Z., Sun, N.-C., Maund, J. R., et al. 2025, ApJL, 987, L10, doi: [10.3847/2041-8213/ade4cd](https://doi.org/10.3847/2041-8213/ade4cd)

Nyholm, A., Sollerman, J., Tartaglia, L., et al. 2020, A&A, 637, A73, doi: [10.1051/0004-6361/201936097](https://doi.org/10.1051/0004-6361/201936097)

Ofek, E. O., Lin, L., Kouveliotou, C., et al. 2013, ApJ, 768, 47, doi: [10.1088/0004-637X/768/1/47](https://doi.org/10.1088/0004-637X/768/1/47)

Ofek, E. O., Cameron, P. B., Kasliwal, M. M., et al. 2007, ApJL, 659, L13, doi: [10.1086/516749](https://doi.org/10.1086/516749)

Ofek, E. O., Sullivan, M., Shaviv, N. J., et al. 2014, ApJ, 789, 104, doi: [10.1088/0004-637X/789/2/104](https://doi.org/10.1088/0004-637X/789/2/104)

Patton, R. A., Kochanek, C. S., & Adams, S. M. 2019, MNRAS, 489, 1986, doi: [10.1093/mnras/stz2282](https://doi.org/10.1093/mnras/stz2282)

Pessi, T., Desai, D. D., Prieto, J. L., et al. 2025, arXiv e-prints, arXiv:2508.10985, doi: [10.48550/arXiv.2508.10985](https://doi.org/10.48550/arXiv.2508.10985)

Quataert, E., & Shiode, J. 2012, MNRAS, 423, L92, doi: [10.1111/j.1745-3933.2012.01264.x](https://doi.org/10.1111/j.1745-3933.2012.01264.x)

Ransome, C. L., Habergham-Mawson, S. M., Darnley, M. J., et al. 2021, MNRAS, 506, 4715, doi: [10.1093/mnras/stab1938](https://doi.org/10.1093/mnras/stab1938)

Ransome, C. L., Habergham-Mawson, S. M., Darnley, M. J., James, P. A., & Percival, S. M. 2022, MNRAS, 513, 3564, doi: [10.1093/mnras/stac1093](https://doi.org/10.1093/mnras/stac1093)

Ransome, C. L., & Villar, V. A. 2025, ApJ, 987, 13, doi: [10.3847/1538-4357/adce03](https://doi.org/10.3847/1538-4357/adce03)

Reguitti, A., Pastorello, A., Pignata, G., et al. 2019, MNRAS, 482, 2750, doi: [10.1093/mnras/sty2870](https://doi.org/10.1093/mnras/sty2870)

Renzo, M., Zapartas, E., de Mink, S. E., et al. 2019, A&A, 624, A66, doi: [10.1051/0004-6361/201833297](https://doi.org/10.1051/0004-6361/201833297)

Richardson, D., Jenkins, III, R. L., Wright, J., & Maddox, L. 2014, AJ, 147, 118, doi: [10.1088/0004-6256/147/5/118](https://doi.org/10.1088/0004-6256/147/5/118)

Riess, A. G., Yuan, W., Macri, L. M., et al. 2022, ApJL, 934, L7, doi: [10.3847/2041-8213/ac5c5b](https://doi.org/10.3847/2041-8213/ac5c5b)

Roming, P. W. A., Pritchard, T. A., Prieto, J. L., et al. 2012, ApJ, 751, 92, doi: [10.1088/0004-637X/751/2/92](https://doi.org/10.1088/0004-637X/751/2/92)

Ryder, S., Staveley-Smith, L., Dopita, M., et al. 1993, ApJ, 416, 167, doi: [10.1086/173223](https://doi.org/10.1086/173223)

Schlafly, E. F., & Finkbeiner, D. P. 2011, ApJ, 737, 103, doi: [10.1088/0004-637X/737/2/103](https://doi.org/10.1088/0004-637X/737/2/103)

Schlegel, E. M. 1990, MNRAS, 244, 269

Schneider, F. R. N., Podsiadlowski, P., & Laplace, E. 2024, A&A, 686, A45, doi: [10.1051/0004-6361/202347854](https://doi.org/10.1051/0004-6361/202347854)

Schröder, S. L., MacLeod, M., Loeb, A., Vigna-Gómez, A., & Mandel, I. 2020, ApJ, 892, 13, doi: [10.3847/1538-4357/ab7014](https://doi.org/10.3847/1538-4357/ab7014)

Schulze, S., Yaron, O., Sollerman, J., et al. 2021, ApJS, 255, 29, doi: [10.3847/1538-4365/abff5e](https://doi.org/10.3847/1538-4365/abff5e)

Senzel, R., Maguire, K., Burgaz, U., et al. 2025, A&A, 694, A14, doi: [10.1051/0004-6361/202451239](https://doi.org/10.1051/0004-6361/202451239)

Shiode, J. H., & Quataert, E. 2014, ApJ, 780, 96, doi: [10.1088/0004-637X/780/1/96](https://doi.org/10.1088/0004-637X/780/1/96)

Silverman, J. M., Nugent, P. E., Gal-Yam, A., et al. 2013, ApJS, 207, 3, doi: [10.1088/0067-0049/207/1/3](https://doi.org/10.1088/0067-0049/207/1/3)

Smith, N. 2017, Philosophical Transactions of the Royal Society of London Series A, 375, 20160268, doi: [10.1098/rsta.2016.0268](https://doi.org/10.1098/rsta.2016.0268)

Smith, N., Andrews, J. E., Filippenko, A. V., et al. 2022, MNRAS, 515, 71, doi: [10.1093/mnras/stac1669](https://doi.org/10.1093/mnras/stac1669)

Smith, N., Andrews, J. E., & Mauerhan, J. C. 2016, MNRAS, 463, 2904, doi: [10.1093/mnras/stw2190](https://doi.org/10.1093/mnras/stw2190)

Smith, N., & Arnett, W. D. 2014, ApJ, 785, 82, doi: [10.1088/0004-637X/785/2/82](https://doi.org/10.1088/0004-637X/785/2/82)

Smith, N., Chornock, R., Li, W., et al. 2008, ApJ, 686, 467, doi: [10.1086/591021](https://doi.org/10.1086/591021)

Smith, N., & Frew, D. J. 2011, MNRAS, 415, 2009, doi: [10.1111/j.1365-2966.2011.18993.x](https://doi.org/10.1111/j.1365-2966.2011.18993.x)

Smith, N., Li, W., Silverman, J. M., Ganeshalingam, M., & Filippenko, A. V. 2011a, MNRAS, 415, 773, doi: [10.1111/j.1365-2966.2011.18763.x](https://doi.org/10.1111/j.1365-2966.2011.18763.x)

Smith, N., & Tombleson, R. 2015, MNRAS, 447, 598, doi: [10.1093/mnras/stu2430](https://doi.org/10.1093/mnras/stu2430)

Smith, N., Li, W., Foley, R. J., et al. 2007, ApJ, 666, 1116, doi: [10.1086/519949](https://doi.org/10.1086/519949)

Smith, N., Miller, A., Li, W., et al. 2010, AJ, 139, 1451, doi: [10.1088/0004-6256/139/4/1451](https://doi.org/10.1088/0004-6256/139/4/1451)

Smith, N., Li, W., Miller, A. A., et al. 2011b, ApJ, 732, 63, doi: [10.1088/0004-637X/732/2/63](https://doi.org/10.1088/0004-637X/732/2/63)

Smith, N., Cenko, S. B., Butler, N., et al. 2012, MNRAS, 420, 1135, doi: [10.1111/j.1365-2966.2011.20104.x](https://doi.org/10.1111/j.1365-2966.2011.20104.x)

Soker, N., & Kashi, A. 2013, ApJL, 764, L6, doi: [10.1088/2041-8205/764/1/L6](https://doi.org/10.1088/2041-8205/764/1/L6)

Sollerman, J., Cumming, R. J., & Lundqvist, P. 1998, ApJ, 493, 933, doi: [10.1086/305163](https://doi.org/10.1086/305163)

Stathakis, R. A., & Stevenson, J. 2001, IAUC, 7782, 3

Stoll, R., Prieto, J. L., Stanek, K. Z., et al. 2011, ApJ, 730, 34, doi: [10.1088/0004-637X/730/1/34](https://doi.org/10.1088/0004-637X/730/1/34)

Sun, N.-C., Maund, J. R., & Crowther, P. A. 2023, MNRAS, 521, 2860, doi: [10.1093/mnras/stad690](https://doi.org/10.1093/mnras/stad690)

Sun, N.-C., de Grijs, R., Subramanian, S., et al. 2017, ApJ, 849, 149, doi: [10.3847/1538-4357/aa911e](https://doi.org/10.3847/1538-4357/aa911e)

Suzuki, A., Moriya, T. J., & Takiwaki, T. 2020, ApJ, 899, 56, doi: [10.3847/1538-4357/aba0ba](https://doi.org/10.3847/1538-4357/aba0ba)

Taddia, F., Stritzinger, M. D., Phillips, M. M., et al. 2012, A&A, 545, L7, doi: [10.1051/0004-6361/201220105](https://doi.org/10.1051/0004-6361/201220105)

Taddia, F., Stritzinger, M. D., Sollerman, J., et al. 2013, A&A, 555, A10, doi: [10.1051/0004-6361/201321180](https://doi.org/10.1051/0004-6361/201321180)

Taddia, F., Sollerman, J., Fremling, C., et al. 2015, A&A, 580, A131, doi: [10.1051/0004-6361/201525989](https://doi.org/10.1051/0004-6361/201525989)

Tang, J., Bressan, A., Rosenfield, P., et al. 2014, MNRAS, 445, 4287, doi: [10.1093/mnras/stu2029](https://doi.org/10.1093/mnras/stu2029)

Thöne, C. C., de Ugarte Postigo, A., Leloudas, G., et al. 2017, A&A, 599, A129, doi: [10.1051/0004-6361/201629968](https://doi.org/10.1051/0004-6361/201629968)

Tsvetkov, D. Y., & Pavlyuk, N. N. 2004, Astronomy Letters, 30, 32, doi: [10.1134/1.1647474](https://doi.org/10.1134/1.1647474)

Van Dyk, S. D., & Matheson, T. 2012, ApJ, 746, 179, doi: [10.1088/0004-637X/746/2/179](https://doi.org/10.1088/0004-637X/746/2/179)

Van Dyk, S. D., Peng, C. Y., Barth, A. J., & Filippenko, A. V. 1999, AJ, 118, 2331, doi: [10.1086/301068](https://doi.org/10.1086/301068)

Van Dyk, S. D., Peng, C. Y., King, J. Y., et al. 2000, PASP, 112, 1532, doi: [10.1086/317727](https://doi.org/10.1086/317727)

van Marle, A. J., Smith, N., Owocki, S. P., & van Veelen, B. 2010, MNRAS, 407, 2305, doi: [10.1111/j.1365-2966.2010.16851.x](https://doi.org/10.1111/j.1365-2966.2010.16851.x)

Wachter, S., Mauerhan, J. C., Van Dyk, S. D., et al. 2010, AJ, 139, 2330, doi: [10.1088/0004-6256/139/6/2330](https://doi.org/10.1088/0004-6256/139/6/2330)

Wagg, T., Dalcanton, J. J., Renzo, M., et al. 2025, arXiv e-prints, arXiv:2504.17903, doi: [10.48550/arXiv.2504.17903](https://doi.org/10.48550/arXiv.2504.17903)

Wang, L., Howell, D. A., Höflich, P., & Wheeler, J. C. 2001, ApJ, 550, 1030, doi: [10.1086/319822](https://doi.org/10.1086/319822)

Woosley, S. E., Blinnikov, S., & Heger, A. 2007, Nature, 450, 390, doi: [10.1038/nature06333](https://doi.org/10.1038/nature06333)

Wu, S., & Fuller, J. 2021, ApJ, 906, 3, doi: [10.3847/1538-4357/abc87c](https://doi.org/10.3847/1538-4357/abc87c)

Wu, S. C., & Fuller, J. 2022, ApJ, 930, 119, doi: [10.3847/1538-4357/ac660c](https://doi.org/10.3847/1538-4357/ac660c)

Xi, Q., Sun, N.-C., Zhao, Y.-H., et al. 2025, MNRAS, 542, 1852, doi: [10.1093/mnras/staf1275](https://doi.org/10.1093/mnras/staf1275)

Xiao, L., Galbany, L., Eldridge, J. J., & Stanway, E. R. 2019, MNRAS, 482, 384, doi: [10.1093/mnras/sty2557](https://doi.org/10.1093/mnras/sty2557)

Xiao, L., Szalai, T., Galbany, L., et al. 2023, arXiv e-prints, arXiv:2312.00562, doi: [10.48550/arXiv.2312.00562](https://doi.org/10.48550/arXiv.2312.00562)

Yoon, S.-C., & Cantiello, M. 2010, ApJL, 717, L62, doi: [10.1088/2041-8205/717/1/L62](https://doi.org/10.1088/2041-8205/717/1/L62)

Zapartas, E., de Mink, S. E., Justham, S., et al. 2021, A&A, 645, A6, doi: [10.1051/0004-6361/202037744](https://doi.org/10.1051/0004-6361/202037744)

—. 2019, A&A, 631, A5, doi: [10.1051/0004-6361/201935854](https://doi.org/10.1051/0004-6361/201935854)

ACKNOWLEDGMENTS

This work is supported by the Strategic Priority Research Program of the Chinese Academy of Sciences, Grant No. XDB05050300, and by the China Manned Space Program with Grant No. CMS-CSST-2025-A14. ZXX is funded by the NSFC Grant No. 12303039. NCS is funded by the NSFC Grants No.12303051 and No. 12261141690. JFL acknowledges support from the NSFC through Grants No. 12588202 and from the New Cornerstone Science Foundation through the New Cornerstone Investigator Program and the XPLORER PRIZE.

We are grateful to Prof. Takashi Moriya for the helpful discussions. ZXX also acknowledges Dr. Andrea Reguitti for kindly providing images of SN 2013gc obtained from NTT, Gemini, and SOAR.

This research has made use of the Keck Observatory Archive (KOA), which is operated by the W. M. Keck Observatory and the NASA Exoplanet Science Institute (NExSci), under contract with the National Aeronautics and Space Administration.

APPENDIX

A. HST LOG

Table A1 presents the archival HST observations used in this paper.

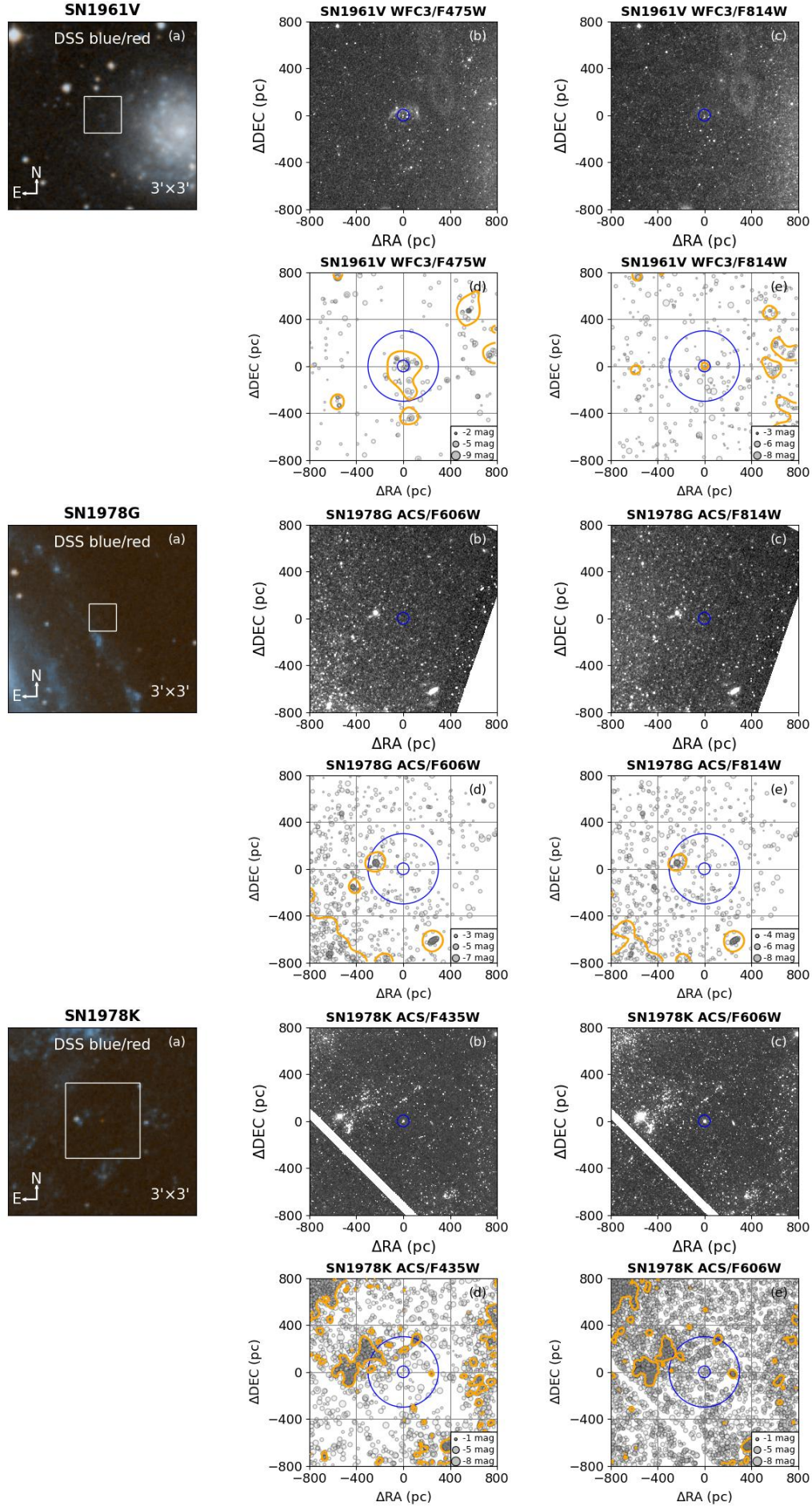
Table A1. HST observations of SNe IIn.

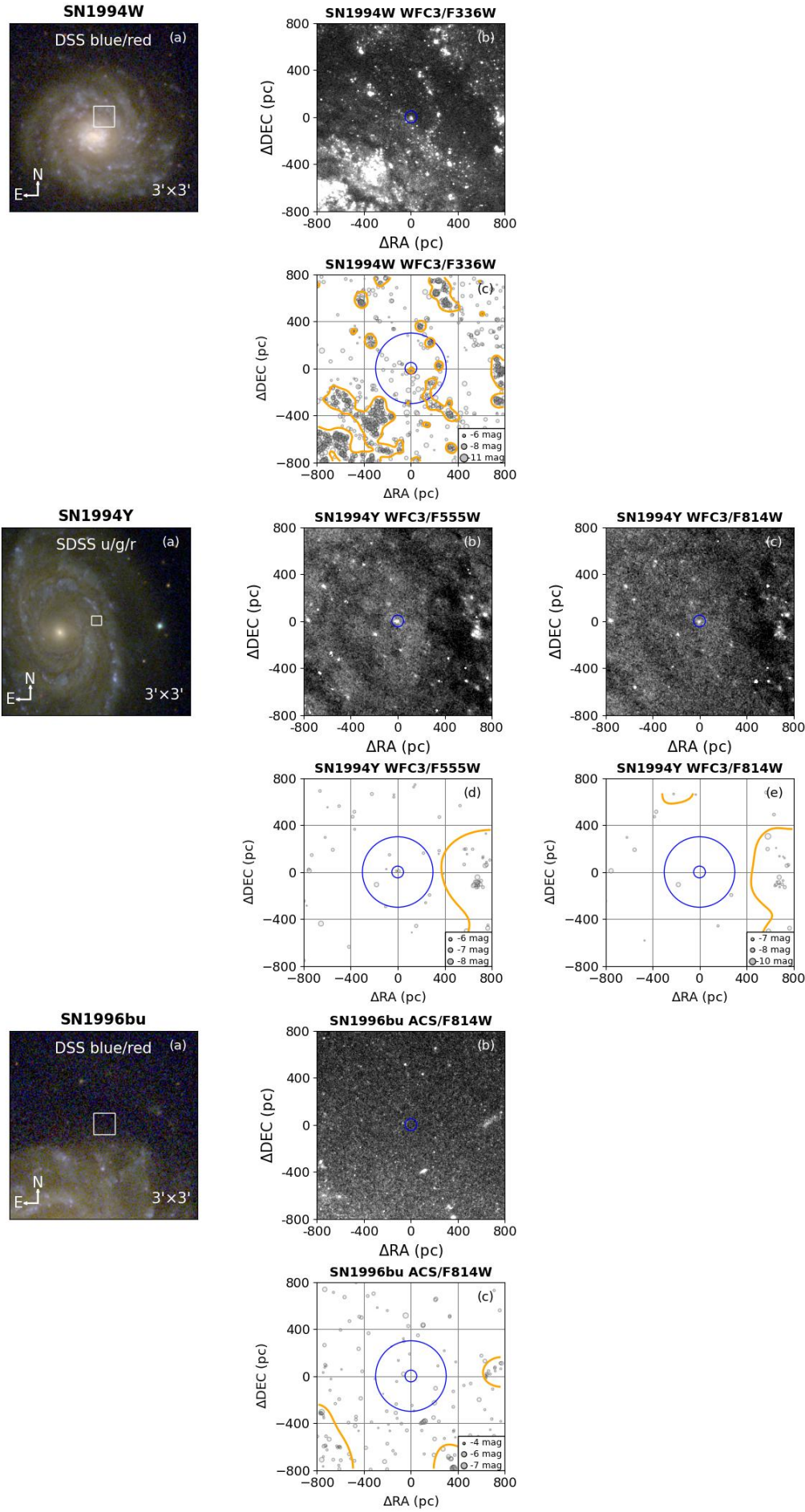
SN	Dataset	Instrument	Program ID	Band	Date(UT)	Exp.Time(s)
SN1961V	IC8502010	WFC3	13477	F475W	2013-12-13	1143
	IC8502020	WFC3	13477	F814W	2013-12-13	1143
SN1978G	JC9V54010	ACS	13442	F606W	2014-05-14	1100
	JC9V54020	ACS	13442	F814W	2014-05-14	1100
SN1978K	JD9G05020	ACS	14786	F435W	2016-09-27	1440
	JD9G05010	ACS	14786	F606W	2016-09-27	1000
SN1994W	ibgt19010	WFC3	12229	F336W	2011-01-30	1800
SN1994Y	IEEC57020	WFC3	16239	F555W	2021-04-07	710
	IEEC57010	WFC3	16239	F814W	2021-04-07	780
SN1996bu	jdxk07010	ACS	15645	F814W	2019-04-24	2304
SN1997bs	ICDM12050	WFC3	13364	F438W	2014-02-08	956
	ICDM12060	WFC3	13364	F555W	2014-02-08	1134
	ICDM12070	WFC3	13364	F814W	2014-02-08	980
SN1997eg	IEEC06020	WFC3	16683	F555W	2021-03-26	710
	IEEC06010	WFC3	16683	F814W	2021-03-26	780
SN1998S	ID9624020	WFC3	14668	F555W	2016-10-03	710
	ID9624010	WFC3	14668	F625W	2016-10-03	780
SN1999el	IERG27020	WFC3	16691	F555W	2022-02-17	710
	IERG27010	WFC3	16691	F814W	2022-02-17	780
SN2000cl	JEY361020	ACS	17070	F555W	2023-11-01	760
	JEY361010	ACS	17070	F814W	2023-11-01	780
SN2003lo	J9NI01011	ACS	10856	F435W	2006-11-08	1000
	J9NI03011	ACS	10856	F555W	2006-11-17	1000
	J9NI04011	ACS	10856	F606W	2006-11-17	1000
	J9NI07011	ACS	10856	F814W	2006-11-19	1000
SN2005gl	ICVY04010	WFC3	14115	F555W	2016-10-17	1194
	ICVY04020	WFC3	14115	F814W	2016-10-17	1194
SN2005ip	IDI112010	WFC3	15166	F336W	2018-01-11	780
	IDI112020	WFC3	15166	F814W	2018-01-11	710
SN2006gy	ICUQ27020	WFC3	14149	F625W	2015-10-10	710

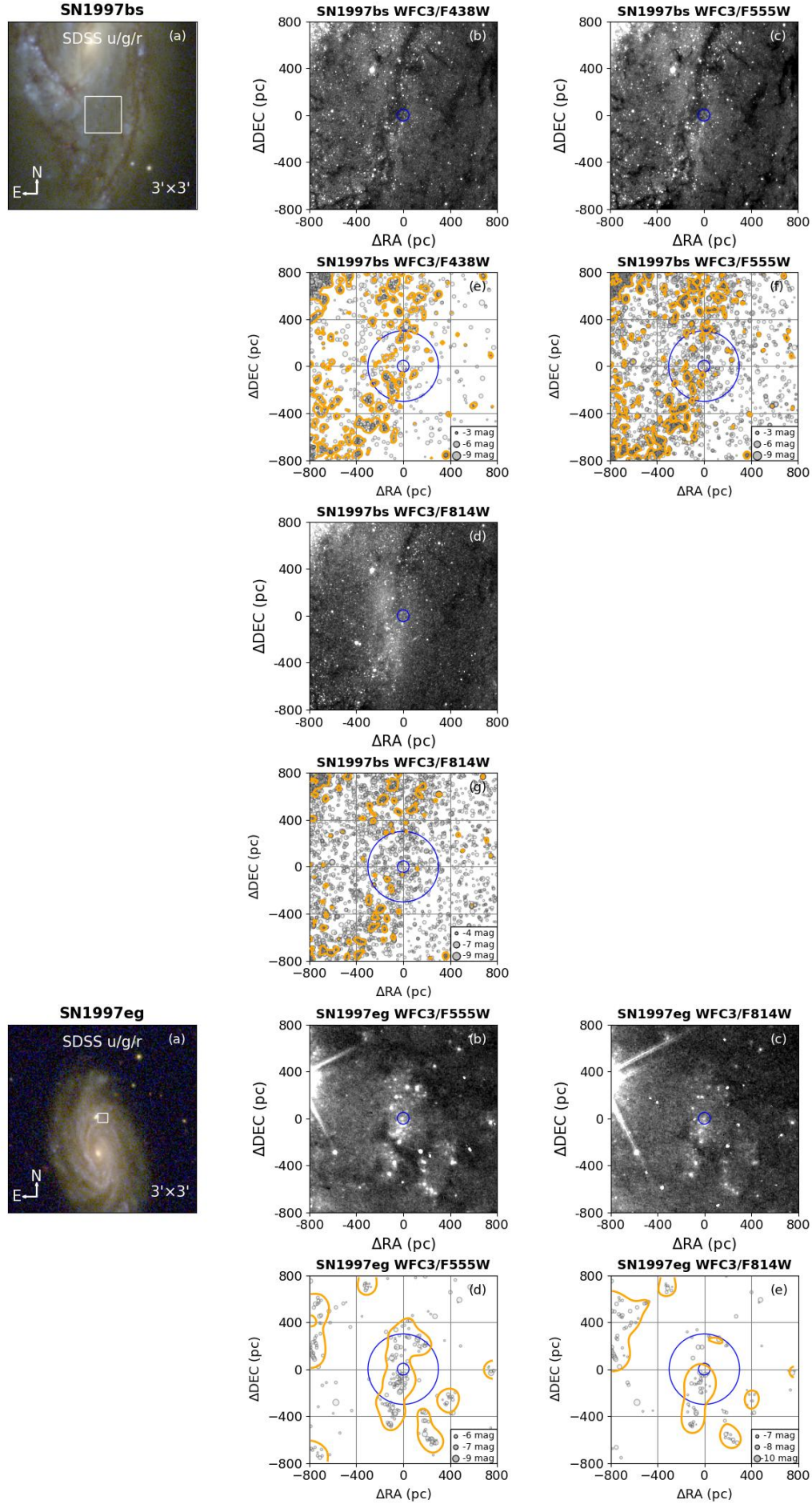
	ICUQ27010	WFC3	14149	F814W	2015-10-10	780
SN2008fq	iebj35010	WFC3	16287	F275W	2021-05-24	1500
SN2009ip	IENP04010	WFC3	16671	F438W	2022-06-05	1061
	IEQE03020	WFC3	16649	F555W	2021-12-14	1034
	IENP04030	WFC3	16671	F606W	2022-06-05	961
	IENP04020	WFC3	16671	F814W	2022-06-05	1061
SN2010bt	JF5569010	ACS	17310	F435W	2024-07-23	674
	JB4U04010	ACS	11575	F606W	2010-10-09	40
	JB4U04020	ACS	11575	F606W	2010-10-09	80
SN2010jj	IERG39020	WFC3	16691	F555W	2022-02-04	710
	IERG39010	WFC3	16691	F814W	2022-02-04	780
SN2010jl	IEB320020	WFC3	16179	F336W	2020-12-29	710
	IEB320010	WFC3	16179	F814W	2020-12-29	780
SN2010jp	ICKJ05010	WFC3	13787	F555W	2015-05-14	4219
	ICKJ05QHQ	WFC3	13787	F814W	2016-05-14	1528
	IBYB10020	WFC3	13029	F625W	2012-12-04	510
	IBYB10010	WFC3	13029	F814W	2012-12-04	680
SN2011ht	ID6U01010	WFC3	14614	F438W	2017-03-10	2932
	ID6U01030	WFC3	14614	F555W	2017-03-10	1386
	ID6U01040	WFC3	14614	F814W	2017-03-10	1386
SN2013gc	IENP03010	WFC3	16671	F438W	2022-03-22	1061
	IEEC52020	WFC3	16239	F555W	2021-10-02	710
	IENP03030	WFC3	16671	F606W	2022-03-22	961
	IENP03020	WFC3	16671	F814W	2022-03-22	1061
SN2014es	jf550m010	ACS	17310	F435W	2025-01-31	674
Gaia14ahl	IDI161020	WFC3	15166	F555W	2019-02-06	710
	IDI161010	WFC3	15166	F814W	2019-02-06	780
SN2015bf	iebjdi010	WFC3	16287	F275W	2021-05-12	1650
SN2015bh	ID9607010	WFC3	14668	F438W	2017-02-17	780
	ID9647020	WFC3	14668	F555W	2017-01-09	710
	ID9607020	WFC3	14668	F625W	2017-02-17	710
	ID9647010	WFC3	14668	F814W	2017-01-09	780
SN2016jbu	IDI141020	WFC3	15166	F555W	2019-03-21	710
	IDI141010	WFC3	15166	F814W	2019-03-21	780
SN2017hcc	iebjao010	WFC3	17770	F275W	2021-08-22	1650
SN2019njv	ifi002010	WFC3	17770	F300X	2025-04-07	1200
SN2021adxl	ifi009010	WFC3	17770	F300X	2025-03-17	1200

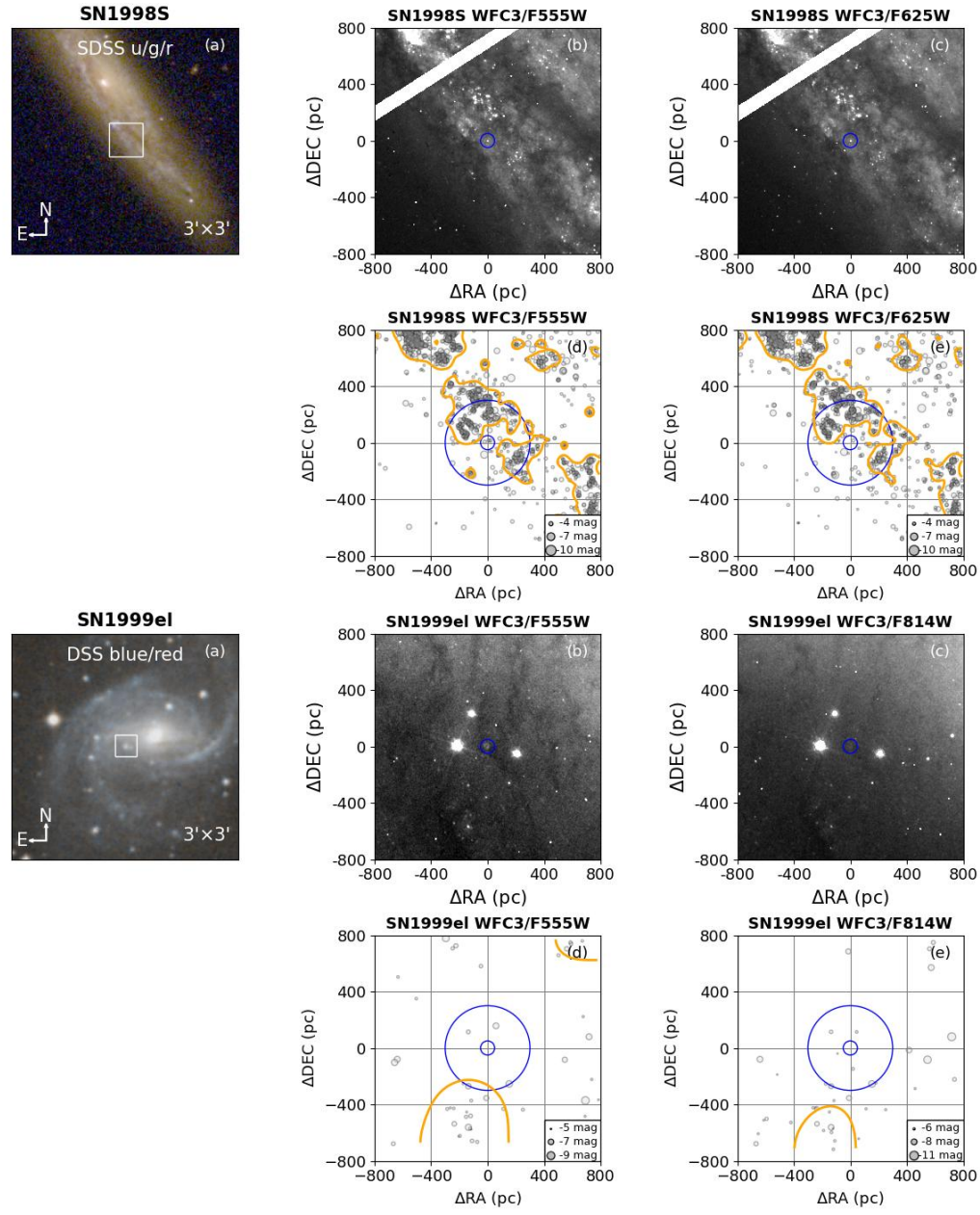
B. SAMPLE ENVIRONMENTS

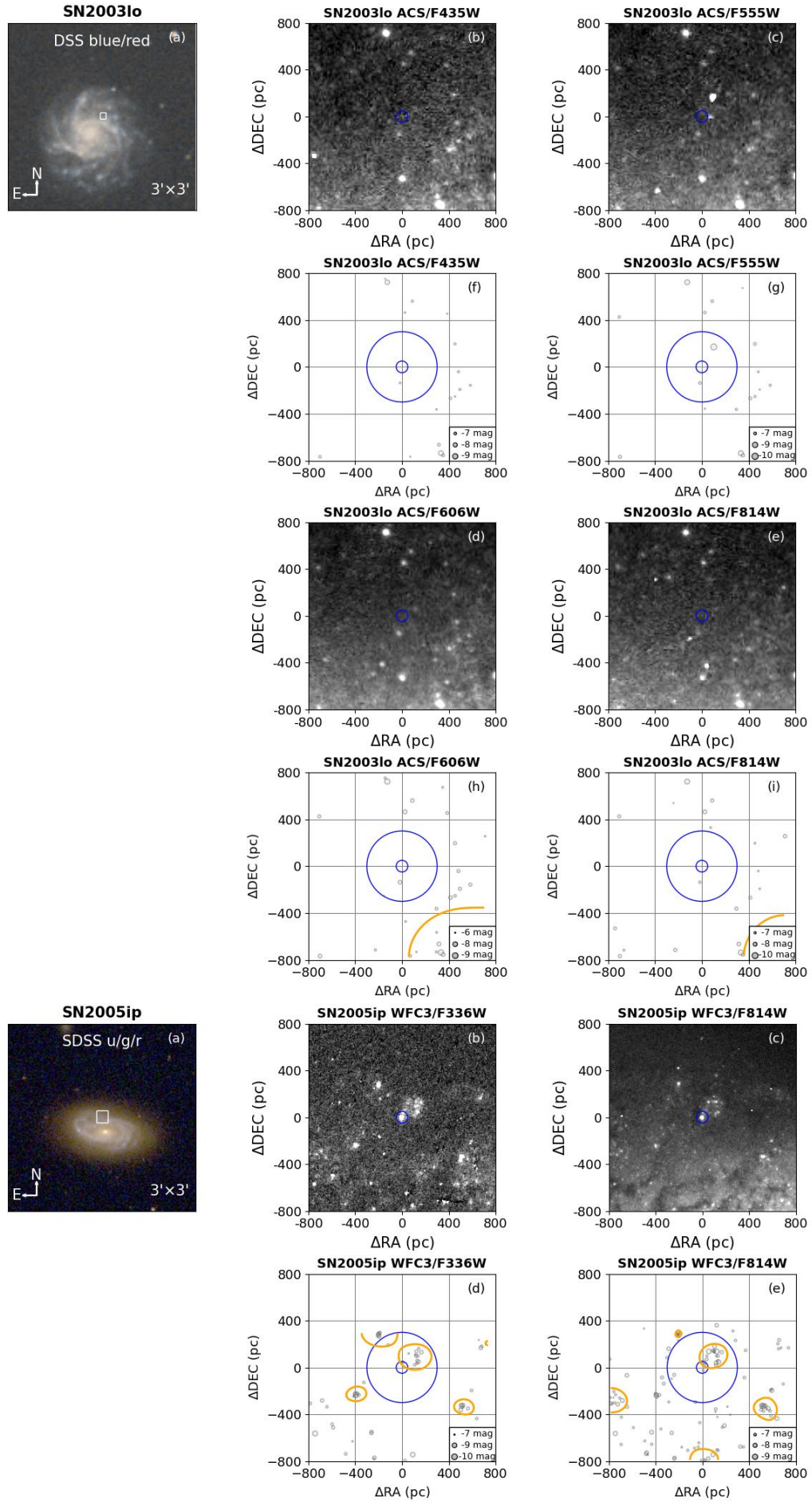
Environmental analysis of other SNe IIn used in this work. The symbols in the images have the same meanings as in Figures 1, 2, and 3. The absence of contours indicates no detection of stellar surface density enhancements. Note that although the environments of SN 2009ip, SN 2010jp, SN 2015bf, Gaia14ahl, and SN 2017hcc are sparse, their classifications were adjusted for other reasons. For details, see Section 4.

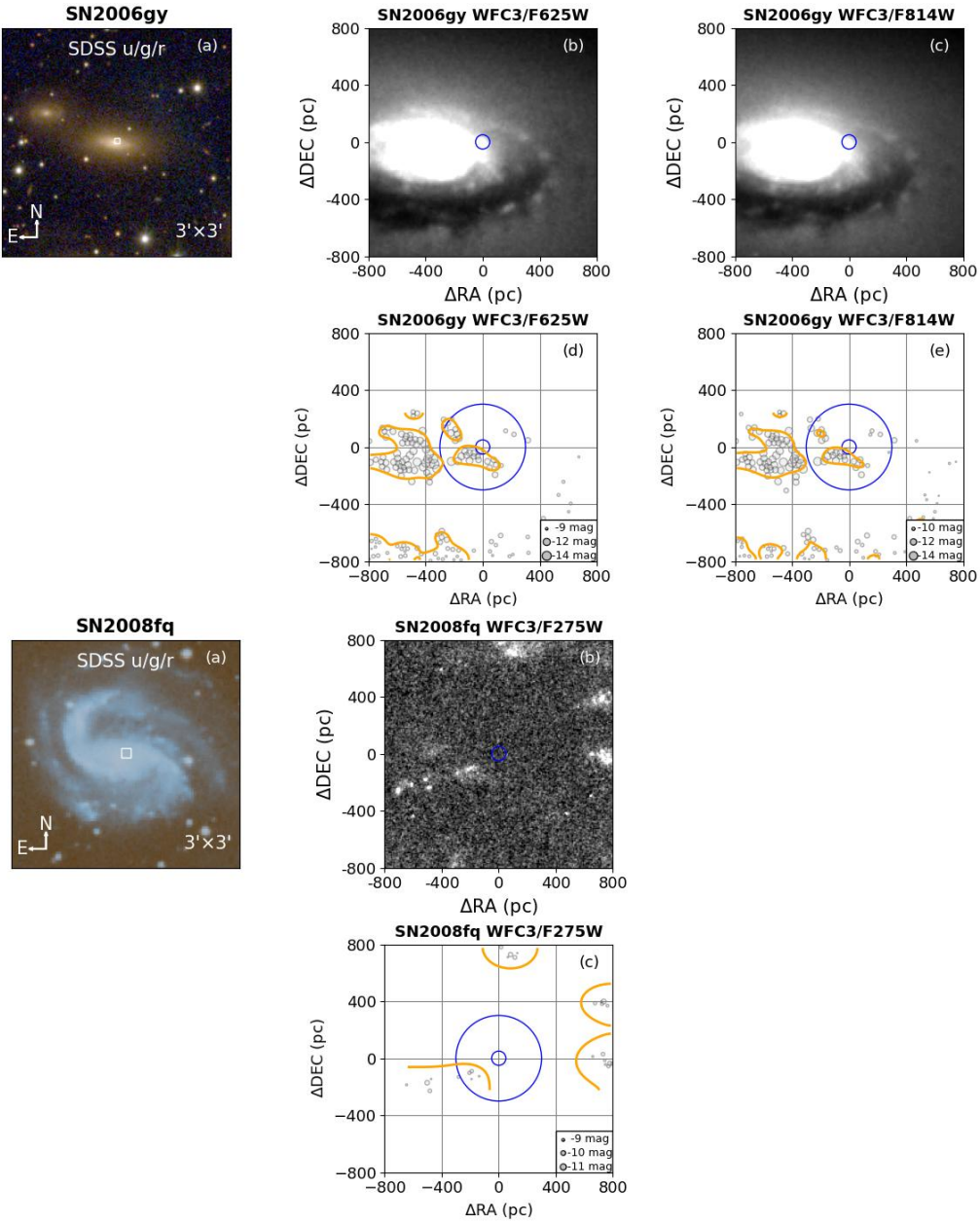


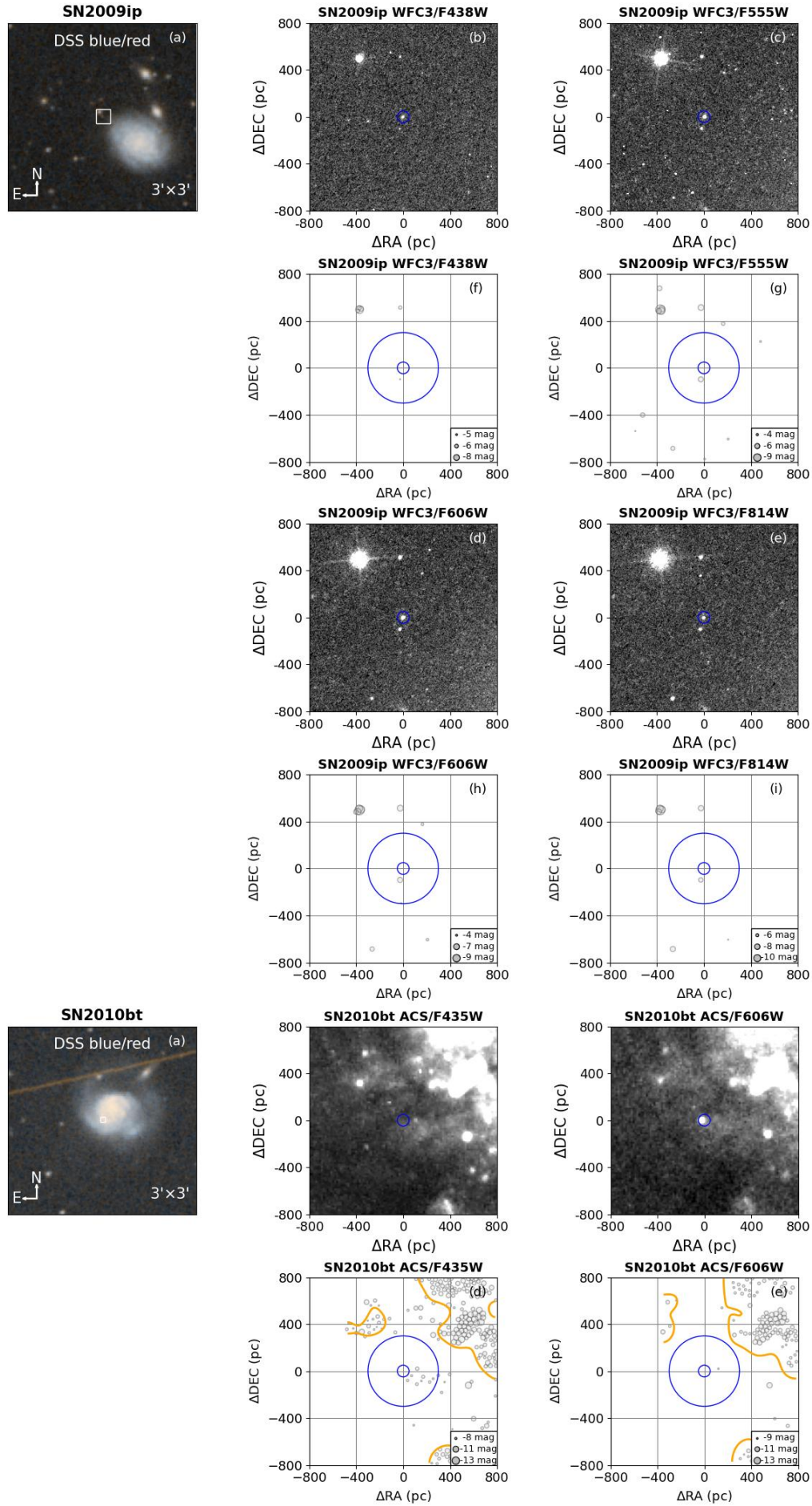


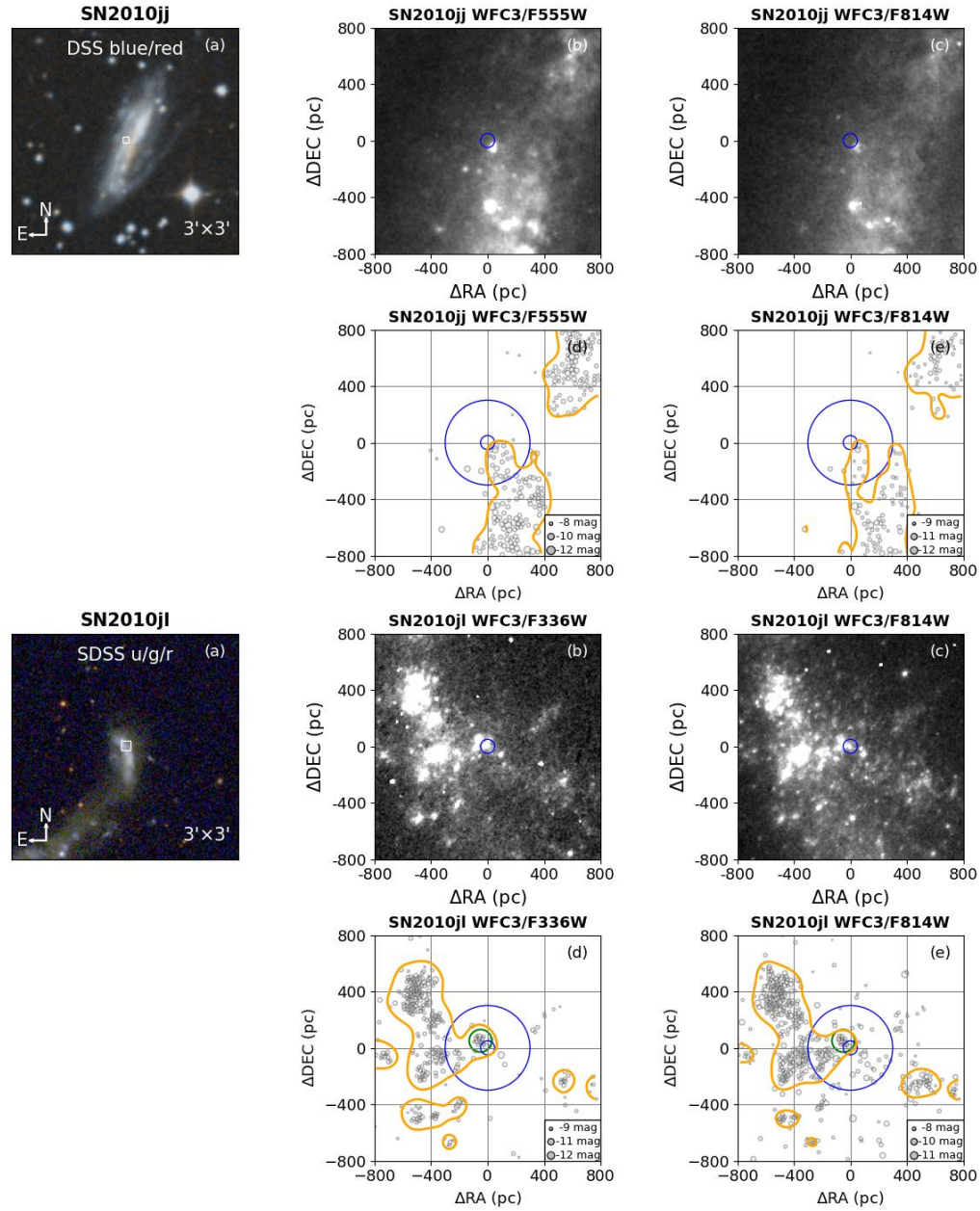


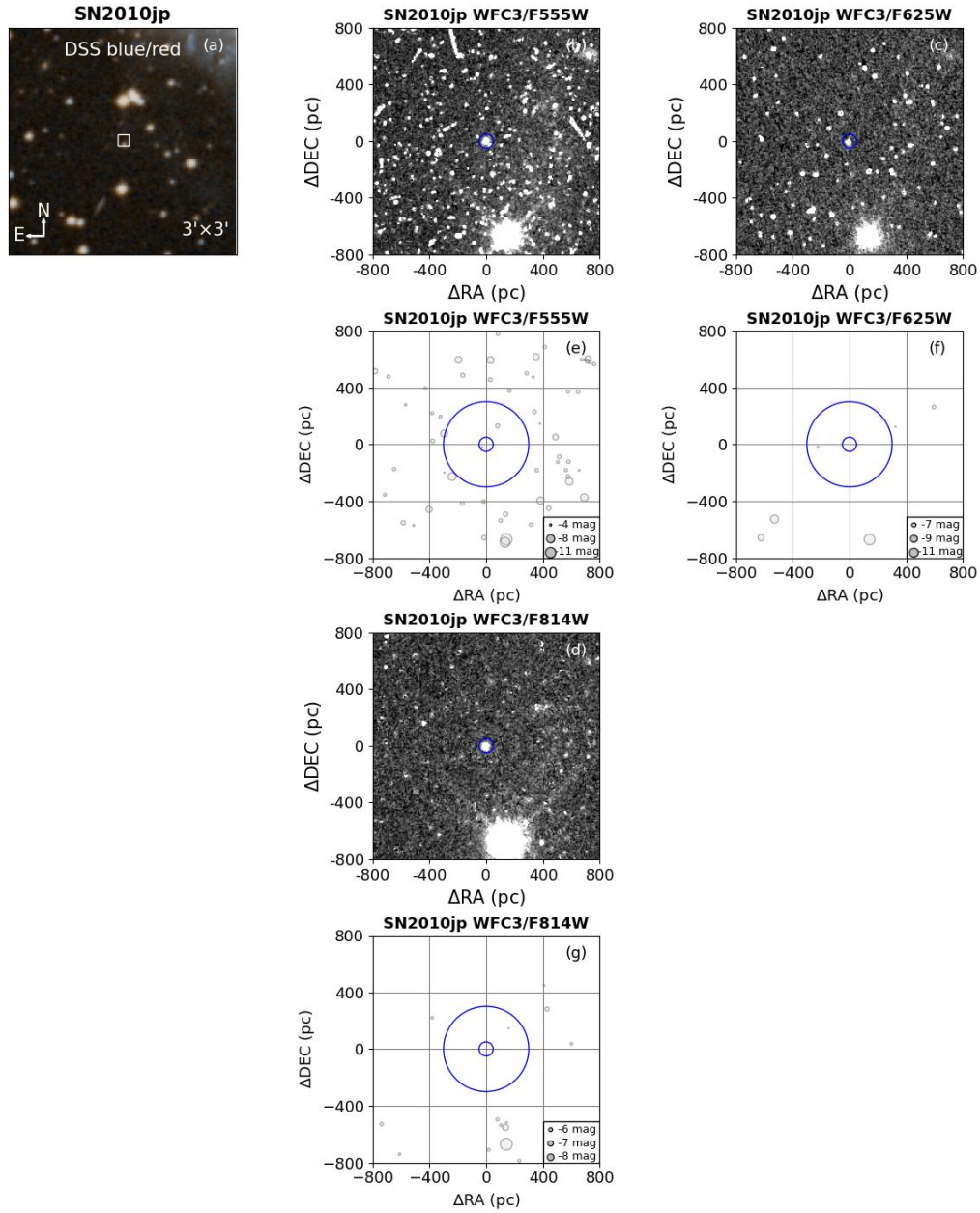


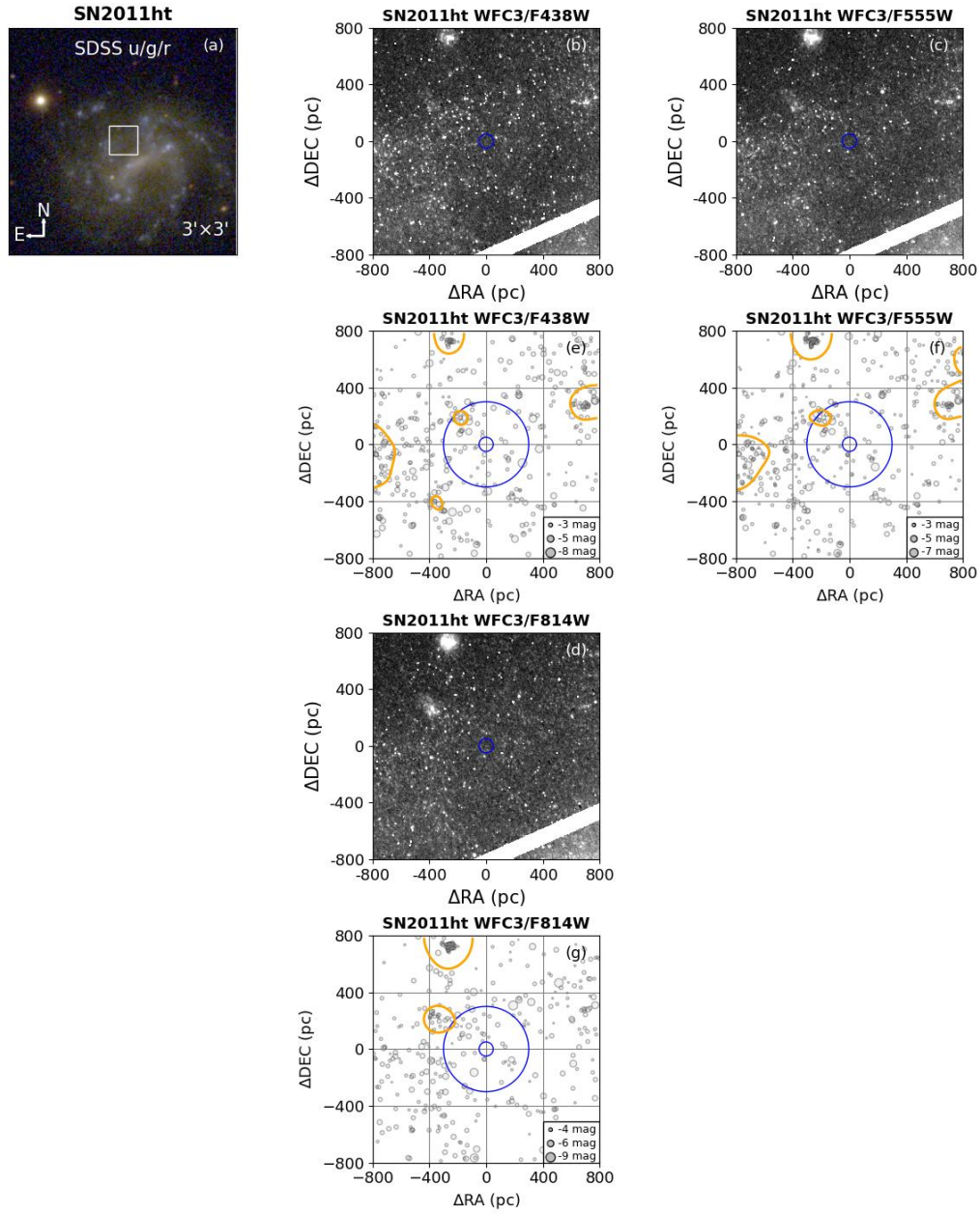


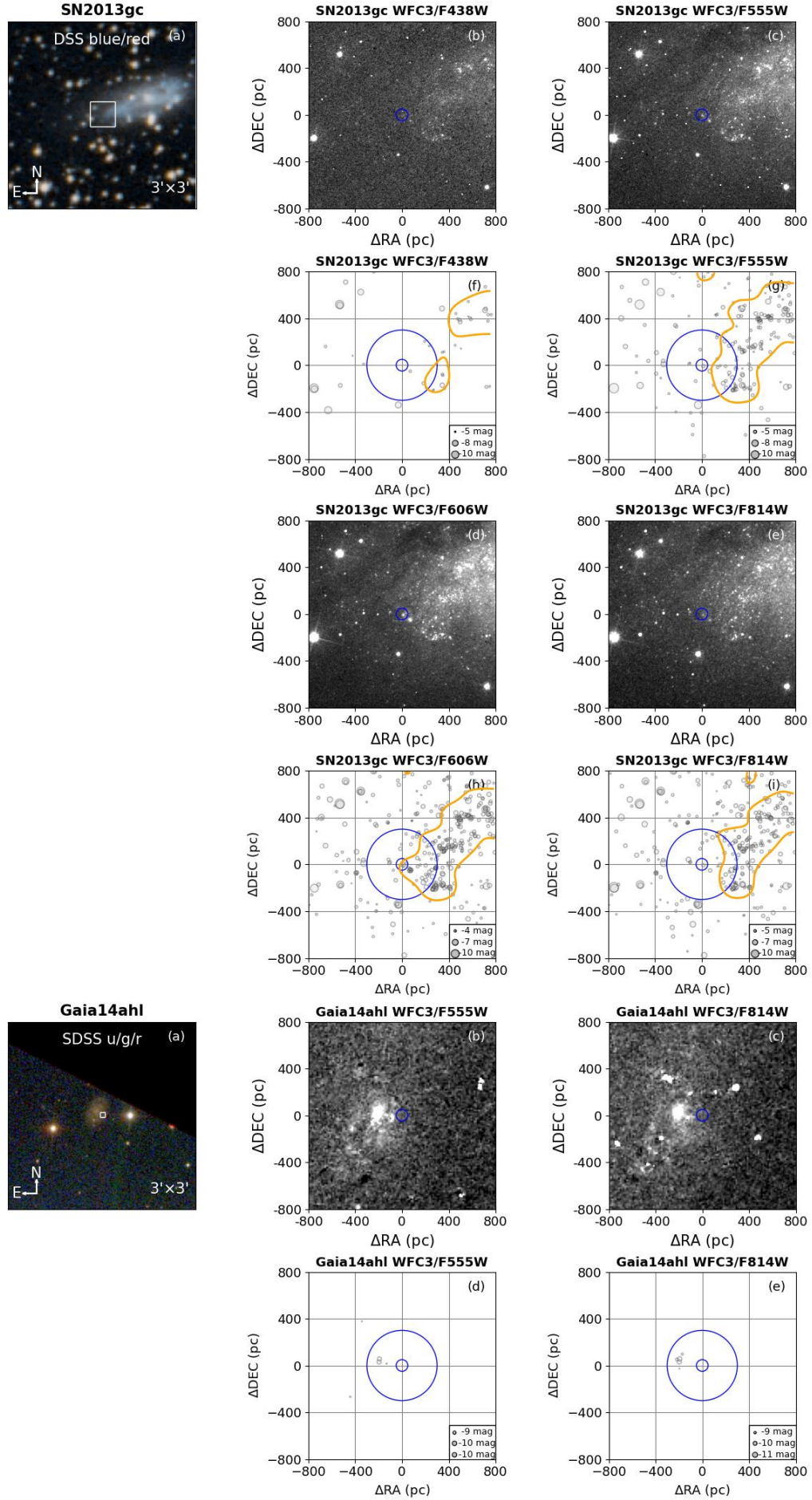


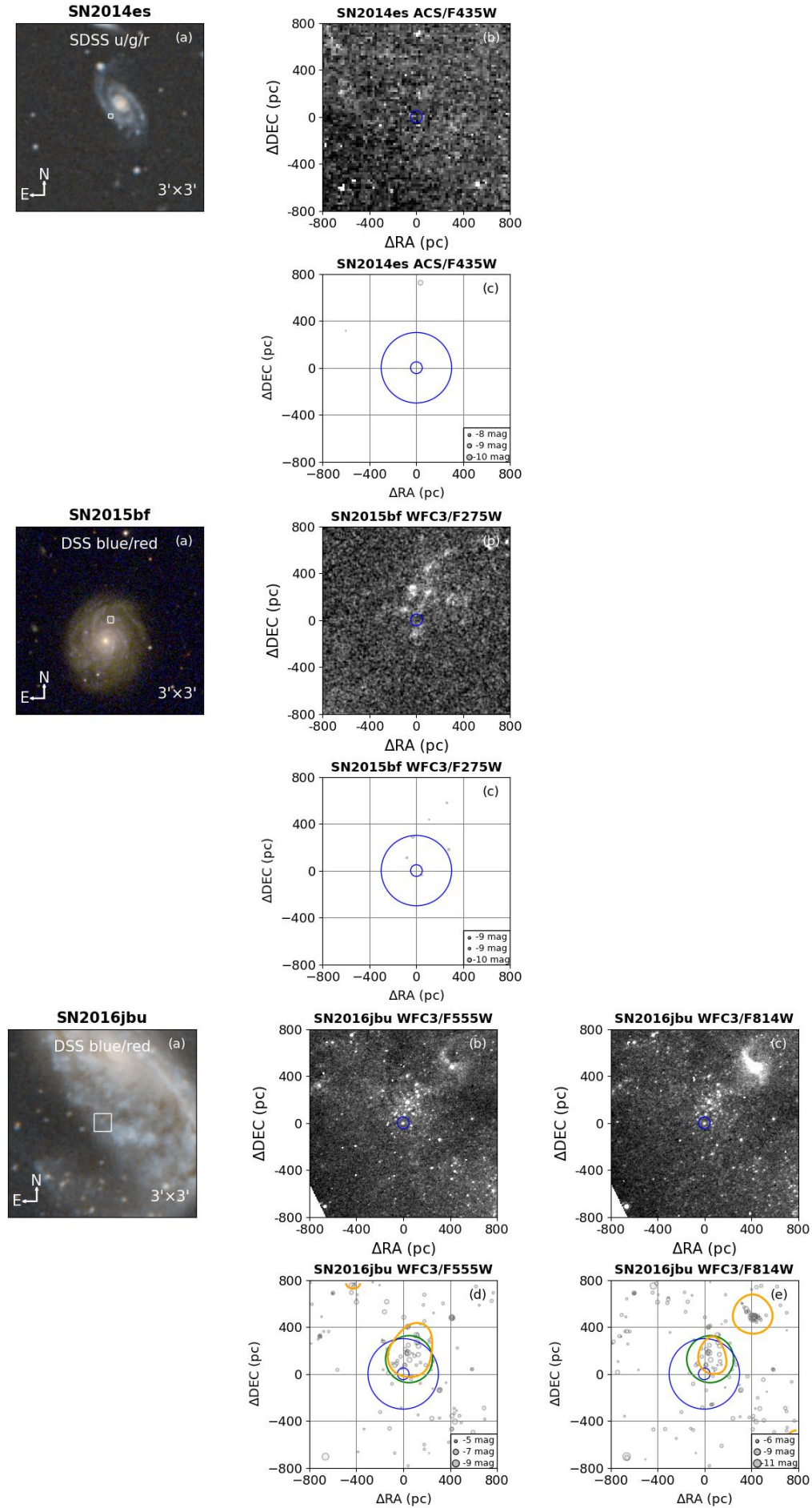












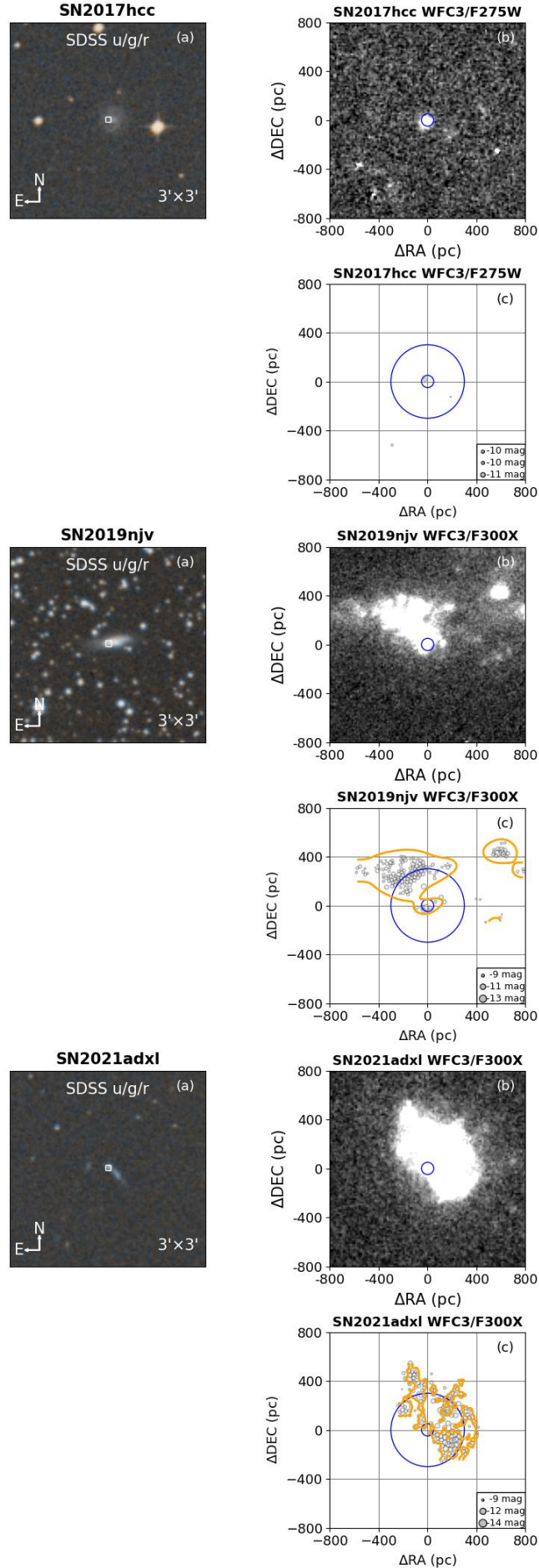


Figure B1. Environmental analysis of other 28 SNe IIn used in this work.

C. PHOTOMETRIC COMPLETENESS

The HST imaging data used in this work were assembled from archival observations spanning varying filters and exposure times. We performed artificial stars tests to quantify the photometric completeness. For SNe with multi-band observations, we convoluted their photometric completeness on the CMD plane with the PARSEC stellar isochrones of given ages and host reddenings. We assumed a total stellar mass of $10^5 M_\odot$ and calculated the number of recovery stars weighted by the adopted initial mass function (IMF) (Kroupa 2002; Kroupa et al. 2013). Generally speaking, redder bands are more sensitive to older stellar population and higher extinction. Therefore, we employed the CMD from the two reddest bands available for each SN to estimate the completeness of the age and reddening. We have tested it with bluer bands and the predicted number of detected stars decreases as expected. For SNe observed in only one band, completeness was derived solely from magnitude distributions. Most of these SNe were observed with UV bands (F300X or F275W), representing the shallowest observations in our sample.

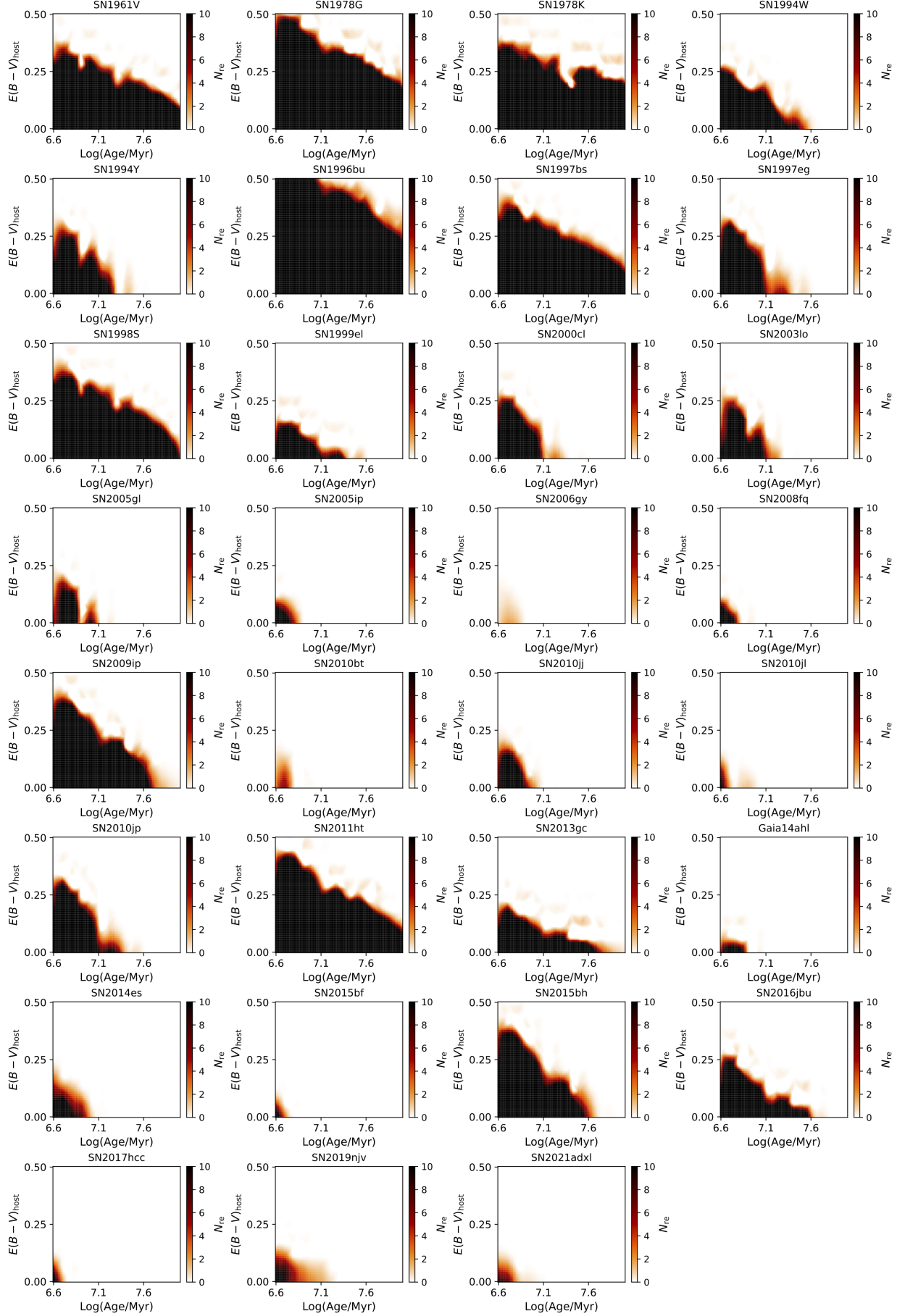


Figure C2. The numbers of recovered star for a $10^5 M_\odot$ stellar population, shown as a function of age and reddening.